

Global Biogeochemical Cycles®



RESEARCH ARTICLE

10.1029/2021GB007121

Relationships Between Air-Sea CO₂ Flux and New Production in the Equatorial Pacific

Nicholas A. Pittman^{1,2} , Peter G. Strutton^{1,2} , Robert Johnson¹ , Richard J. Matear³ , and Adrienne J. Sutton⁴

¹Institute for Marine and Antarctic Studies, University of Tasmania, Hobart, TAS, Australia, ²Australian Research Council Center of Excellence for Climate Extremes, University of Tasmania, Hobart, TAS, Australia, ³Commonwealth Scientific and Industrial Research Organisation, Hobart, TAS, Australia, ⁴Pacific Marine Environmental Laboratory, National Oceanic and Atmospheric Administration, Seattle, WA, USA

Key Points:

- Decadal shifts in upwelling have increased CO₂ flux in the cold tongue but not biological production, which is likely nutrient limited
- Increasing frequency of central Pacific El Niño events may amplify decadal CO₂ flux trends and drive sink conditions in the west
- Increasing surface temperatures contribute to stratification and decreasing new production despite increasing dissolved inorganic carbon

Correspondence to:

N. A. Pittman,
nic.pittman@utas.edu.au

Citation:

Pittman, N. A., Strutton, P. G., Johnson, R., Matear, R. J., & Sutton, A. J. (2022). Relationships between air-sea CO₂ flux and new production in the equatorial Pacific. *Global Biogeochemical Cycles*, 36, e2021GB007121. <https://doi.org/10.1029/2021GB007121>

Received 21 JUL 2021
Accepted 16 MAR 2022

Author Contributions:

Conceptualization: Nicholas A. Pittman, Peter G. Strutton
Funding acquisition: Peter G. Strutton
Methodology: Nicholas A. Pittman, Peter G. Strutton, Robert Johnson, Richard J. Matear, Adrienne J. Sutton
Project Administration: Peter G. Strutton
Software: Nicholas A. Pittman
Supervision: Peter G. Strutton, Robert Johnson, Richard J. Matear
Visualization: Nicholas A. Pittman
Writing – original draft: Nicholas A. Pittman
Writing – review & editing: Nicholas A. Pittman, Peter G. Strutton, Robert Johnson, Richard J. Matear, Adrienne J. Sutton

Abstract The equatorial Pacific is the largest oceanic source of carbon dioxide to the atmosphere. This outgassing varies depending on the El Niño–Southern Oscillation (ENSO) and decadal climate variability. New production, the amount of phytoplankton net primary production driven by upwelled nitrate, plays a significant role in modulating air-sea CO₂ fluxes as the biological carbon pump removes carbon from the surface ocean. We aim to understand how the physical drivers of sea surface temperature and wind speed influence interannual and decadal variability of the equatorial Pacific carbon cycle. In the equatorial Pacific, there are three biogeochemical regimes: the upwelling cold tongue east of 140°W and south of the equator (3°N–15°S); the eastern Pacific warm pool north of the equator (3°–15°N); and the 28.5°C western Pacific warm pool, west of 140°W. We find that between 2000 and 2020, air-sea CO₂ flux and Δ*p*CO₂ increased in the cold tongue (45 mmolC m⁻² yr⁻², 1.5 μatm yr⁻¹, respectively) but decreased elsewhere, while new production decreased everywhere. The western Pacific occasionally became a weak carbon sink, depending on ENSO and this sink was strongest at 165°E during central Pacific “Modoki” El Niño events. We find that changes in wind speed, temperature and ENSO frequency have altered the surface carbon budget. The mean basin-wide (150°E–90°W and 15°N–15°S) new production for 2000–2020 was 1.2 ± 0.1 PgC yr⁻¹ and air-sea CO₂ flux was 0.5 ± 0.1 PgC yr⁻¹. New production decreased at -7.7 ± 1.6 TgC yr⁻², compared to the CO₂ flux trend of -1.7 ± 1.4 TgC yr⁻².

Plain Language Summary The equatorial Pacific is the largest source of carbon dioxide that outgasses from the ocean into the atmosphere. This outgassing varies depending on the El Niño–Southern Oscillation (ENSO) and decadal changes in the climate. Winds in the eastern Pacific drive upwelling which supplies nutrients and carbon to the surface. Some of this carbon is outgassed to the atmosphere, some is consumed by phytoplankton and can either move through the food web or sink into the ocean interior. We are interested in how much carbon is removed from the surface equatorial Pacific through outgassing of carbon and biological consumption. We find that changes in wind speeds, surface temperatures, freshening surface water and changing patterns of ENSO have influenced the equatorial Pacific carbon budget. For example, between 2000 and 2020, CO₂ release to the atmosphere increased in the upwelling zone but decreased elsewhere, while biological consumption decreased everywhere. The western Pacific occasionally absorbs carbon from the atmosphere during central Pacific “Modoki” El Niño events, a particular type of El Niño that is becoming more frequent.

1. Introduction

The equatorial Pacific Ocean (15°N–15°S and 150°E–90°W) is the largest oceanic source of carbon dioxide (CO₂) to the atmosphere, releasing an average of 0.5 PgC (petagrams of carbon, 10¹⁵gC) annually between 10°N and 10°S annually (F. Chavez et al., 1999; Takahashi et al., 1997). The eastern Pacific (EP) CO₂ source has increased since the 1980s due to increases in both the surface partial pressure of carbon dioxide (*p*CO₂) and wind speeds (Landschützer et al., 2016; Sutton, Feely, et al., 2014; Wanninkhof & Triñanes, 2017; Yasunaka et al., 2019). Increasing *p*CO₂ has been attributed to more entrainment from subtropical surface waters on decadal timescales, and raising oceanic CO₂ faster than atmospheric concentrations in the EP, although slower in the western Pacific (Sutton, Feely, et al., 2014). Air-sea CO₂ flux, defined here as outgassing from the ocean into the atmosphere, has been studied extensively throughout the equatorial Pacific and a number of gridded *p*CO₂

© 2022 The Authors.

This is an open access article under the terms of the [Creative Commons Attribution-NonCommercial License](https://creativecommons.org/licenses/by-nc/4.0/), which permits use, distribution and reproduction in any medium, provided the original work is properly cited and is not used for commercial purposes.

and CO₂ flux products are available for analysis (Iida et al., 2015; Ishii et al., 2014; Landschützer et al., 2016; Takahashi et al., 1997; Yasunaka et al., 2019).

The equatorial Pacific is also a region of globally significant primary and new production. New production is the amount of phytoplankton net primary production (NPP) fueled by upwelled (“new”) nitrate (Falkowski et al., 2003). New production plays a significant role in air-sea CO₂ fluxes, because the biological carbon pump or export flux, removes carbon from the surface ocean (Bennington et al., 2009; DeVries et al., 2012; McKinley et al., 2017; Pennington et al., 2006; Strutton & Chavez, 2000). New production accounts for 0.65–0.98 PgC yr⁻¹ exported from the surface ocean between 90°W and 180°, 5°N and 5°S (F. P. Chavez et al., 1996). No published decadal new production trends are available for the equatorial Pacific. However chlorophyll, as a proxy for phytoplankton biomass, is a good indicator of both NPP and new production, and has decreased at between 0.33% and 1.30% decade⁻¹ since 2000 (Pittman et al., 2019). The equatorial Pacific Ocean Climate Studies in the 1980s and Joint Global Ocean Flux Study in the 1990s provided a comprehensive database of new production (Aufdenkampe et al., 2001; F. P. Chavez & Barber, 1987; Le Borgne, Feely, & Mackey, 2002; Murray et al., 1994; Quay, 1997). Additional new production data became available through follow-up studies, but none after the early 2000s (Sabine et al., 2004; Strutton et al., 2004). A number of global satellite-based primary production (Behrenfeld et al., 2005; Eppley, 1972; Morel, 1991; Silsbe et al., 2016; Westberry et al., 2008) and new production models are available (Dunne et al., 2005; Henson et al., 2010; Laws et al., 2000, 2011; Siegel et al., 2014). There have been few specific analysis of these products in the equatorial Pacific. However, in the EP cold tongue and western Pacific warm pool (WPWP), interannual variability of export flux is large with a standard deviation that is about 70% of the average annual export (Dunne et al., 2007).

The equatorial Pacific can be separated into distinct biogeochemical provinces: the south-eastern, north-eastern, and western equatorial Pacific (Le Borgne, Barber, et al., 2002; Le Borgne & Rodier, 1997; Longhurst, 2007; Pennington et al., 2006; Radenac et al., 2013). The south-eastern equatorial cold tongue and Peruvian upwelling, herein called the cold tongue is defined by the 25°C isotherm, roughly 3°N–15°S, and is characterized by upwelled cool, dissolved inorganic carbon (DIC)- and nutrient-rich water (Fiedler & Talley, 2006; Wyrski, 1981). Upwelled DIC is either outgassed to the atmosphere, consumed by biology alongside nutrients, or advected away from the equator by wind-driven Ekman transport (Landry et al., 1997; Liao et al., 2020). North of the equator lies the eastern Pacific Warm Pool (EPWP; 3°–15°N), which includes the Gulfs of Tehuantepec, Papagayo, and Panama, and is characterized by highly stratified waters and warm sea surface temperatures (SSTs; Fiedler & Talley, 2006; Pennington et al., 2006; Wyrski, 1981). The WPWP is defined by the 28.5°C isotherm, and is relatively fresh, stratified and its longitudinal extent varies considerably at seasonal and interannual time scales, reaching between 170°W in boreal summer and 130°E in boreal winter (Cravatte et al., 2009; Le Borgne, Barber, et al., 2002; Radenac et al., 2013).

Air-sea CO₂ flux and new production vary at seasonal, interannual and decadal timescales (F. Chavez et al., 1999; Feely et al., 2002; Takahashi et al., 1997). Both new production and air-sea CO₂ flux are typically largest in the EP, and decrease toward the west and away from the equator. The largest driver of temporal variability is the El Niño-Southern Oscillation (ENSO), which influences tropical Pacific air-sea CO₂ fluxes and new production by impacting three main processes: thermocline depth, trade-wind strength and cold tongue extent (Feely et al., 2002; McKinley et al., 2004; McPhaden et al., 2006). CO₂ outgassing and new production are reduced during El Niño and are elevated during La Niña (F. Chavez et al., 1999). The difference between *p*CO₂ in the ocean and atmosphere (Δp CO₂; ocean minus atmosphere) in the EP can reach over 200 ppm during La Niña events, causing significant outgassing (Feely et al., 2006; Strutton et al., 2008; Sutton, Feely, et al., 2014; Takahashi et al., 2002). In contrast, strong El Niño events can drive Δp CO₂ below 0 ppm in the central and western equatorial Pacific (~140°W to 165°E), temporarily causing a weak sink for atmospheric CO₂ (F. Chavez et al., 1999; Sutton, Feely, et al., 2014; Takahashi et al., 2002). During EP “canonical” El Niño events, new production is depressed in the eastern equatorial Pacific and elevated west of 180°W when compared with neutral conditions (Strutton & Chavez, 2000; Turk et al., 2001, 2011). Central Pacific (CP) “Modoki” El Niño events have become more frequent relative to EP events since the 1990s (Ashok et al., 2007; Cai, Santoso, et al., 2015; Freund et al., 2019; Marathe et al., 2015; T. Lee & McPhaden, 2010), and have been shown to reduce new production and CO₂ flux in the western Pacific, but are similar to neutral conditions in the EP (Gierach et al., 2012; Liao et al., 2020; Messié & Chavez, 2013; Racault et al., 2017; Turk et al., 2011; Valsala et al., 2014). The majority

of export variability here is at interannual scales, emphasizing the impact of ENSO on new production and the carbon budget (Dunne et al., 2007).

Here, we use over 20 years of satellite- and mooring-based physical and biogeochemical observations of the equatorial Pacific. They include satellite and shipboard productivity and temperature data, and surface ocean observations of temperature, wind speed and $p\text{CO}_2$ from six TAO-TRITON equatorial moorings (F. P. Chavez et al., 1998; Sutton, Feely, et al., 2014). Until now, no climate-scale studies have combined these data to assess the variability of new production and air-sea CO_2 flux relative to each other. Here, we combine a gridded CO_2 product and satellite derived new production alongside mooring observations to answer the following questions:

1. What are the decadal trends of new production and air-sea CO_2 flux? How are they related in the equatorial Pacific?
2. What is the relationship between new production and CO_2 flux in the different phases of ENSO?

2. Methods and Data

2.1. Mapped $p\text{CO}_2$ and Air-Sea CO_2 Flux

Monthly, 1° global gridded (Landschützer et al., 2014, 2016, 2020) $p\text{CO}_2$ and air-sea CO_2 flux products (2020 reprocessing), herein referred to as Landschützer, were used throughout this analysis (https://www.nodc.noaa.gov/ocads/oceans/SPCO2_1982_present_ETH_SOM_FFN.html, downloaded August 2020). The Landschützer product spans 1982–2020, uses data from the Surface Ocean CO_2 Atlas Version 2, including data from the TAO/TRITON moorings, and interpolates these data to a 1° grid using the ETH-SOM-FFN method (self-organizing map and a feed-forward network). The interpolation method uses SST, sea surface salinity, mixed layer depth, chlorophyll-a and climatological sea surface $p\text{CO}_2$ from Takahashi et al. (2009). Positive CO_2 fluxes indicate that CO_2 is outgassed into the atmosphere.

2.2. Primary Production Estimates

Four NPP models were obtained from <http://sites.science.oregonstate.edu/ocean.productivity> (accessed August 2020): CAFE (Carbon, Absorption, and Fluorescence Euphotic-resolving model; Silsbe et al., 2016), VGPM (Vertically Generalized Production Model; Morel, 1991), Eppley-VGPM (Eppley, 1972; Morel, 1991), and CbPM (Carbon-based Production Model (Behrenfeld et al., 2005; Westberry et al., 2008)). These products were regridded using Python xESMF (<https://doi.org/10.5281/zenodo.1134365>) from 0.1° to 1° to be consistent with the air-sea CO_2 flux products. We used a first-order conservative spatial averaging method which averages the mean of all source grid boxes.

2.3. New Production Estimates

New production is the fraction of NPP that is fueled by upwelled nitrate (NO_3) as opposed to recycled ammonium (NH_4). We assume that new production and carbon export are equivalent when averaged at spatial scales of about 1,000 km and seasonal time scales in the tropical Pacific Ocean (Dugdale & Goering, 1967; Eppley & Peterson, 1979; Falkowski et al., 2003; Plattner, 2005; Sarmiento & Gruber, 2006). The f -ratio is the ratio of new production to total NPP. Several authors have provided estimates of the f -ratio or vertical POC fluxes and equations to calculate the biological export of carbon out of the upper ocean (DeVries & Weber, 2017; Dunne et al., 2005; Henson et al., 2011; Laws et al., 2000, 2011). For simplicity, we refer to all of these algorithms as new production, however this may overestimate export flux due to missing the lateral advection component of the carbon budget (Landry et al., 1997). The time-series depicted here were calculated from the equations in each paper, except the SIMPLE-TRIM models (DeVries & Weber, 2017), which were obtained from <https://tdevries.eri.ucsb.edu/models-and-data-products/> (downloaded August 2020). We calculated the mean (climatology) and one standard deviation of the 12 SIMPLE-TRIM models. f -ratio calculations generally use a polynomial relationship between SST and NPP, which is then multiplied by NPP to estimate new production. Laws et al. (2011) provides two f -ratio formulations, where their Equation 2 (called L2011a here) is based on nitrogen uptake in the surface, and their Equation 3 (called L2011b here) is based on a combination of global particle export measurements as well as nitrogen uptake. The f -ratio for (Dunne et al., 2005) was calculated using the Z. Lee et al. (2007) monthly euphotic depth products for SeaWiFS and MODIS-Aqua, and was regridded to 1° . This euphotic depth

data set was provided by NASA Ocean Biology Processing Group, Greenbelt, MD, USA, and maintained by NASA Ocean Biology Distributed Active Archive Center, accessed March 2021 (NASA Goddard Space Flight Center, Ocean Ecology Laboratory, Ocean Biology Processing Group, 2018a, 2018b). The regridded 1° models were compared with published values to decide on the most accurate model combination of NPP algorithm and f -ratio to use.

2.4. Physical, Biological, and Climate Data Sets

The Reynolds 1° monthly Optimal Interpolation Sea Surface Temperature (OISST; Reynolds et al., 2002) product was provided by the NOAA/OAR/ESRL PSL, Boulder, Colorado, USA, from their website <https://psl.noaa.gov/data/gridded/data.noaa.oisst.v2.html>, downloaded August 2020. The OISST was used to calculate f -ratios for the new production algorithms. Temperature profiles from the surface to 200 m were obtained for six equatorial TAO-TRITON moorings at 165°E, 170°W, 155°W, 140°W, 125°W, and 110°W, accessed from the NOAA National Data Buoy Centre (NDBC, https://tao.ndbc.noaa.gov/tao/data_download/search_map.shtml, downloaded January 2020). Ocean and atmospheric $p\text{CO}_2$ and surface winds were obtained to calculate CO_2 flux for the equatorial moorings between 2004 and 2019 from PMEL (Pacific Marine Environmental Laboratory; Sutton, Sabine, et al., 2014; Sutton et al., 2019) <https://www.ncei.noaa.gov/access/ocean-carbon-data-system/oceans/Moorings/Pacific.html> and <https://www.pmel.noaa.gov/co2/timeseries/>, downloaded October 2020). This CO_2 flux data was used for comparison with the Landschützer product. The Tropical Pacific Chlorophyll Algorithm (TPCA; Pittman et al., 2019) was accessed from <https://researchdata.edu.au/tropical-pacific-chlorophyll-reprocessing-v10/1438905> (downloaded January 2020). Monthly 0.25° wind speeds were obtained for the Cross-Calibrated Multi-Platform (CCMP) product Version 2 due to its superior performance in the equatorial Pacific (Chiodi et al., 2019). CCMP (Wentz et al., 2015) was obtained from <http://www.remss.com/measurements/ccmp/>, downloaded January 2021. This product was regridded to 1° using xESMF as per NPP.

2.5. Analysis and Timescale Methods

A kernel density estimate was used to calculate the frequency distribution of new production and CO_2 flux. To calculate trends from monthly averaged data, 60 rolling, 17 years linear regressions were performed, staggered by month and spanning 1998–01 to 2002–12 through 2015–01 to 2019–12. These are referred to as mean rolling trends. The intention of using the mean of 60 rolling 17 years trends rather than using single regression was to understand the influence of interannual variability, and time series start and end points on this short 22 years time-series. To reduce the number of panels in figures, we discuss but do not show the standard deviation. It is expressed as a % of the total trend and is referred to as trend sensitivity, and significant trends are indicated with stippling. These trends were calculated at the mooring locations, and for each pixel on spatial maps. Maps of the Pearson correlation coefficient (r^2) for each variable and time were produced. Significant trends were defined where p -values were <0.05 . Two sample independent t -tests were performed on maps of ENSO anomalies compared with neutral conditions to identify significant ($p < 0.05$) differences. January 2000 was chosen as the start date for calculating trends, to eliminate any potential influence of the 1997–1998 El Niño. Annual new production rates were calculated for the area integrated between 150°E and 100°W, 10°N and 10°S. A cross-correlation lag analysis was performed on the full new production and air-sea CO_2 flux time series for each mooring, and between adjacent moorings. New production and air-sea flux were correlated at between –6 and +6 months lag to one another to identify relationships between them. Correlations were also performed on pairs of variables, and also their linearly detrended time series.

This research used open source data sets and processing libraries. Python 3.7 was used for the analysis, using Numpy, Scipy, Pandas, and xarray. The full source code to reproduce this analysis is available at <https://doi.org/10.5281/zenodo.5120943>.

2.6. Classifying ENSO

The Multivariate ENSO Index v2 (MEI) was downloaded from <https://www.esrl.noaa.gov/psd/enso/mei/> (August 2020). The EMI (El Niño Modoki Index; Ashok et al., 2007) estimates were downloaded from http://www.jamstec.go.jp/virtualearth/data/SINTEX/SINTEX_EMI.csv (August 2020, offline as of January 2022 but available via their email). CP El Niño events were classified by an EMI ≥ 0.5 for five consecutive months. EP events were

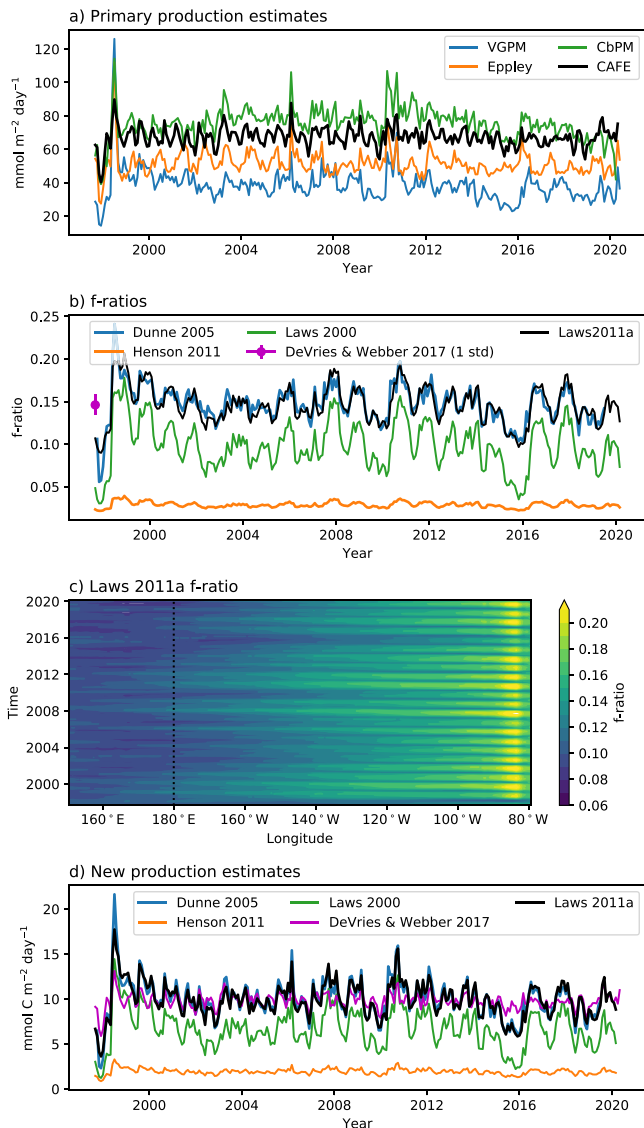


Figure 1. (a) Four satellite derived net primary production (NPP) algorithm estimates at 0°N 140°W . Expected NPP values are between 58 and 75 $\text{mmolC m}^{-2} \text{day}^{-1}$ (F. Chavez et al., 1999). (b) Five f -ratio estimates at 0°N 140°W . Values of between 0.1 and 0.25 are expected (F. P. Chavez et al., 1996; McCarthy et al., 1996; Strutton et al., 2004). The model selected for this analysis is L2011a in black. The magenta point is the SIMPLE-TRIM (DeVries & Weber, 2017) climatology with 1 standard deviation shown. (c) Hovmöller plot of the L2011a f -ratio, 1997–2019, averaged from 15°N to 15°S . (d) New production at 0°N 140°W for the five f -ratio estimates multiplied by CAFE primary production. Expected new production values are between 10 and 20 $\text{mmolC m}^{-2} \text{day}^{-1}$.

classified by an MEI ≥ 0.5 for 5 months and not co-located with a CP event during December, January or February. La Niña was classified as any five consecutive months with an MEI ≤ -0.5 .

3. Results

3.1. New Production Model Selection

Selecting optimal NPP and f -ratio models was challenging due to a lack of POC flux or nitrate uptake measurements in the equatorial Pacific during the satellite era. Therefore, we compared four satellite-based NPP products at 140°W (Figure 1a) in order to inform our choice. CAFE is the best performing model across global in situ NPP data (K. Bisson et al., 2020; K. M. Bisson et al., 2018; Kahru, 2017; Silsbe et al., 2016). At 140°W , in situ NPP estimates range between approximately 58.3 and 75.0 $\text{mmolC m}^{-2} \text{day}^{-1}$ (F. P. Chavez et al., 1996; Le Borgne, Feely, & Mackey, 2002; Lefèvre et al., 1994; Strutton et al., 2004). CAFE averages 67.2 $\text{mmolC m}^{-2} \text{day}^{-1}$ throughout the satellite record, and was selected for use here. The averages for the other models were 39.8 $\text{mmolC m}^{-2} \text{day}^{-1}$ for VGPM, 52.0 $\text{mmolC m}^{-2} \text{day}^{-1}$ for Eppley and 76.0 $\text{mmolC m}^{-2} \text{day}^{-1}$ for CbPM.

We compared five f -ratio estimates in Figure 1b. At 140°W , the overall mean f -ratios for these models were 0.03 for Henson et al. (2011), 0.10 for Laws et al. (2000), 0.14 for L2011a, 0.15 for Dunne et al. (2005) and $0.15 (\pm 0.01)$ for SIMPLE-TRIM, where the standard deviation is based on the 12 model members. In-situ f -ratios in this region range between 0.04 and 0.46 with a mean of approximately 0.15 (Aufdenkampe et al., 2001, 2002; F. P. Chavez et al., 1996; McCarthy et al., 1996; Murray et al., 1994; Strutton et al., 2004; Turk et al., 2011). The L2011a model fits this mean well and provides similar estimates to both Dunne et al. (2005) and the SIMPLE-TRIM climatology (DeVries & Weber, 2017). L2011a was one of the best performing models in the global analysis of Li and Cassar (2016), so we used it with the CAFE model to calculate new production for the rest of our analysis.

The L2011a f -ratio is presented through time for 150°E – 80°W , averaged from 15°N – 15°S in Figure 1c. The f -ratio ranges between 0.08 in the western Pacific and 0.22 in the east, with a mean of 0.12 . The f -ratio increase toward the east is consistent with shipboard observations (Aufdenkampe et al., 2001; Turk et al., 2011). At 140°W , mean new production is 9.9 $\text{mmolC m}^{-2} \text{day}^{-1}$ (Figure 1d), slightly lower than the 13.5 – 20.3 $\text{mmolC m}^{-2} \text{day}^{-1}$ found by Chavez et al. (1996), but they used f -ratios of 0.18 – 0.27 , higher than is expected (Le Borgne, Feely, & Mackey, 2002). On the other end of the spectrum, Le Borgne, Feely, and Mackey (2002) calculated an average value of 9.6 $\text{mmolC m}^{-2} \text{day}^{-1}$ for their export flux at 140°W , which is toward the lower end of the estimates here. DeVries and Weber (2017) SIMPLE-TRIM, Dunne et al. (2005) and the selected L2011a model have similar magnitudes, but vary in regard to seasonal and interannual variability. However, it must be noted that the SIMPLE-TRIM model has no seasonal or interannual variability due to it being a steady-state model climatology

(DeVries & Weber, 2017). Henson et al. (2011) is low compared with the other estimates because it is based on particle flux at 100 m, which may be biased due to some shallow remineralization. However the general inter-annual variability of NPP, f -ratio and New Production are similar for the different approaches (Figures 1a, 1b and 1d; DeVries & Weber, 2017; Siegel et al., 2014).

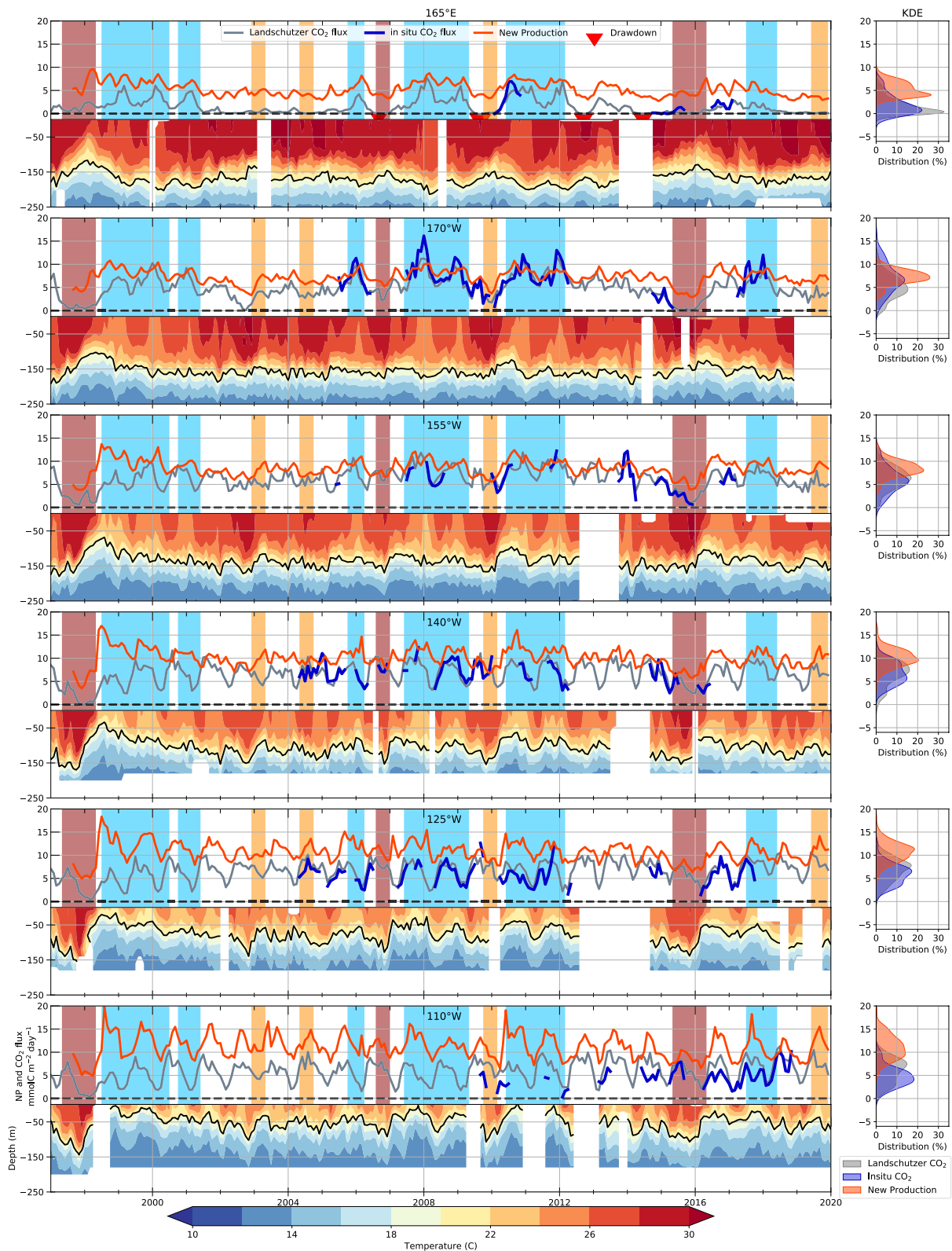


Figure 2.

3.2. Air-Sea CO₂ Flux, New Production and Upper Ocean Temperature Temporal Patterns at the Mooring Locations

The largest air-sea CO₂ flux mean is 6.3 ± 2.4 mmolC m⁻² day⁻¹ at 140°W. It decreases toward the east and west and ranges from 1.6 ± 1.6 mmolC m⁻² day⁻¹ at 165°E to 5.3 ± 2.6 mmolC m⁻² day⁻¹ at 110°W (Figure 2). Mean new production increases west to east, from 5.3 ± 1.6 mmolC m⁻² day⁻¹ at 165°E to 11.0 ± 2.6 mmolC m⁻² day⁻¹ at 110°W (Figure 2). In general, the air-sea CO₂ flux estimates of Landschützer et al. (2014, 2016) are similar in magnitude and variability to in situ air-sea CO₂ flux observations, and are within $\pm 15\%$ mean absolute percentage error of the mooring fluxes, except the east Pacific is 69% overestimated, likely due to the poor observational record here (Figure 2), Landschützer underestimates in situ mooring observations by -0.7 mmolC m⁻² day⁻¹ at 170°W and overestimates observations by 2.2 mmolC m⁻² day⁻¹ at 110°W. Good coherence between these two products is expected as the mooring data is assimilated in the Landschützer interpolation, and is confirmed by the distribution plots (Figure 2, right hand side).

Air-sea CO₂ flux and new production have a complex relationship with ENSO, but generally peak during or soon after La Niña events, particularly in the west when stratification is weak (170°W, Figure 2). During and following El Niño events, basin-wide new production is suppressed by 10.3% (Table 1), followed by a rapid increase at all locations (Figure 2). The equatorial Pacific Ocean becomes a weaker CO₂ source during strong EP and CP El Niño events and a stronger source during La Niña. The western Pacific (165°E) CO₂ flux is small, except during La Niña events. This location infrequently becomes a weak CO₂ sink. This has occurred for 8 months total in the 20 years considered here (small red triangles in Figure 2). The average drawdown of these events is 0.058 mmolC m⁻² day⁻¹, which is $\sim 3\%$ of the mean flux at this location. These sink periods occurred before the 2007 CP and 2010 EP El Niño events, and also during boreal summer and autumn during neutral conditions in 2012 and 2014. The temperature time series (Figure 2) confirms that El Niño causes warmer upper ocean temperatures and a shallower 20°C isotherm, compared to cooler surface temperatures and strong upwelling during La Niña. Thermocline shoaling during La Niña occurs together with increases in both new production and CO₂ flux. At 165°E, the 20°C isotherm shoaled significantly at 0.48 ± 0.16 m yr⁻¹ between 2000 and 2020 (Figure 2). At 125°W, the 20°C isotherm deepened at -0.53 ± 0.24 m yr⁻¹, and everywhere else the thermocline changes are not statistically significant.

The seasonal variability of new production and CO₂ flux is largest in the EP, and weakens toward the west (Figure 2). SST is warmest at 110°W during March and April (boreal spring, weaker winds), and cools until August, decreasing by over 3.5°C in four months. At 165°E, the peak in temperature occurs between September and November (boreal fall) and the magnitude of the seasonal cycle is less than 1°C. New production in the east is lowest during April and highest during August and September. Air-sea CO₂ flux varies similarly. It's minimum in March and maximum is in July (not shown). At 165°E, the largest peaks in new production occur in March and to a lesser extent in October. Seasonality of $\Delta p\text{CO}_2$ is similar to that of new production, ranging between 95 μatm in May and 70 in December.

3.3. Spatial Patterns and Decadal Trends of Carbon, Biological, and Physical Variables

For the analysis in this section, 17 years rolling trends between the initial start dates of 1998–2002 and end dates of 2015–2020, were used to quantify the decadal trend and its uncertainty.

The SST decadal trend increased significantly throughout the equatorial Pacific at an average of $0.016^\circ\text{C yr}^{-1}$ (Figure 3b). Trend sensitivity, that is 1 standard deviation of the mean rolling trends, was about 50% of the mean 17-year trend in the cold-tongue, but close to 100% near the dateline, which is the largest sensitivity of any variable (not shown, Figure 3 stippling indicate significant trends). The WPWP (defined by the 28.5°C isotherm) expanded toward the east between 2000–2005 and 2015–2020, from near the 165°E mooring to the 170°W mooring (Figure 3a). The location of the 25°C isotherm (dashed line), which defines the cold tongue, was correlated with spatial patterns in other variables. Wind speeds were largest in the south-east where they are south-easterly in the central northern Equatorial Pacific where they are typically north-easterly (Figure 3c). The mean rolling trends

Figure 2. Air-sea CO₂ flux and Carbon, Absorption, and Fluorescence Euphotic-resolving model (CAFE) × L2011a new production for six mooring locations (1° pixel) across the Pacific. Red lines are new production. Gray lines are Landschützer CO₂ flux, Blue lines are in situ CO₂ flux from moorings when available. Vertical shaded bars indicate eastern Pacific El Niño (red), central Pacific El Niño (orange), and La Niña (blue) events persisting for at least 5 months. Red triangles are months when CO₂ flux was into the ocean. Bottom panels show temperature as a function of time and depth and the black contour is the 20°C isotherm depth. Right hand side shows the frequency distribution of the three products as a percentage, with the same y-axis and data as the left hand-side in mmolC m⁻² day⁻¹. The area of each distribution integrates to 100.

Table 1

Overview Statistics for the Western, Central, and Eastern Regions and the Entire Tropical Pacific Basin 2000–2020 Area Integrations in PgC, as Shown by the Black Boxes in Figure 3k

Region (15°N–15°S)	West (165°–180°W)	Central (155°–140°W)	East (125°–110°W)	Basin (150°E–90°W)
Area (10 ⁶ km ²)	5.49	5.49	5.49	43.79
NP mean (PgC yr ⁻¹)	0.105	0.159	0.193	1.213
NP neutral (PgC yr ⁻¹)	0.098	0.154	0.190	1.178
NP EP El Niño (PgC yr ⁻¹)	0.100	0.130	0.166	1.058
NP CP El Niño (PgC yr ⁻¹)	0.097	0.149	0.197	1.187
NP La Niña (PgC yr ⁻¹)	0.117	0.176	0.204	1.303
NP EP El Niño diff (% PgC yr ⁻¹)	2.0%, 0.002	-15.6%, -0.024	-12.6%, -0.024	-10.2%, -0.120
NP CP El Niño diff (% PgC yr ⁻¹)	-1.0%, -0.001	-3.2%, -0.005	3.7%, 0.007	0.8%, 0.009
NP La Niña diff (% PgC yr ⁻¹)	19.4%, 0.019	14.3%, 0.022	7.4%, 0.014	10.6%, 0.125
NP trends (TgC yr ⁻²)	-0.916 ± 0.19	-0.843 ± 0.25	-1.305 ± 0.30	-7.659 ± 1.56
NP trends (% yr ⁻²)	-0.873%	-0.53%	-0.676%	-0.631%
NP <i>p</i> -value	3.2 × 10 ⁻⁵	7.2 × 10 ⁻³	5.2 × 10 ⁻³	2.4 × 10 ⁻⁴
CO ₂ mean (PgC yr ⁻¹)	0.014	0.070	0.095	0.459
CO ₂ neutral (PgC yr ⁻¹)	0.008	0.069	0.097	0.448
CO ₂ EP El Niño (PgC yr ⁻¹)	0.003	0.038	0.072	0.290
CO ₂ CP El Niño (PgC yr ⁻¹)	0.002	0.060	0.097	0.417
CO ₂ La Niña (PgC yr ⁻¹)	0.028	0.082	0.097	0.531
CO ₂ EP El Niño diff (% PgC yr ⁻¹)	-62.5%, -0.005	-44.9%, -0.031	-25.8%, -0.025	-35.3%, -0.158
CO ₂ CP El Niño diff (% PgC yr ⁻¹)	-75.0%, -0.006	-13.0%, -0.009	0.0%, 0.0	-6.9%, -0.031
CO ₂ La Niña diff (% PgC yr ⁻¹)	250.0%, 0.02	18.8%, 0.013	0.0%, 0.0	18.5%, 0.083
CO ₂ trends (TgC yr ⁻²)	-0.473 ± 0.21	-0.281 ± 0.29	0.281 ± 0.27	-1.730 ± 1.41
CO ₂ trends (% yr ⁻²)	-3.3%	-0.40%	0.295%	-0.377%
CO ₂ <i>p</i> -value mean	0.130	0.120	0.460	0.158
CO ₂ <i>p</i> -value median	0.040	0.087	0.499	0.069

Note. Trends are the 17-year mean rolling trends. For new production (NP) and air-sea CO₂ flux, we compared all time mean, neutral mean, El Niño mean, La Niña mean, El Niño difference from neutral (in percent and Pg, El Niño minus neutral), La Niña difference from neutral (in % and PgC, La Niña minus neutral), trends, percent change and *p*-values of the mean rolling trends. Uncertainty is 1 standard error. Red bold mean increases and blue bold means decreases. Note that the Trends are in TgC rather than PgC (PgC = 10¹⁵gC and TgC = 10¹²gC).

here are uncertain, where only a few locations in the eastern and central northern Pacific changed significantly, however increased and became more southerly in the cold tongue region but converged and decreased significantly in the central region north of the equator around 115°W, 4°N (Figure 3d). There is also high uncertainty between different wind speed products in the equatorial Pacific (Chiodi et al., 2019; Roobaert et al., 2018). TPCA chlorophyll (Figure 3e) is largest in the cold tongue and decreases toward the west. Chlorophyll spatial variability is similar to new production and decreased between 2000 and 2020, except in the cold tongue and a small region in the western Pacific around 165°E (Figure 3f). Chlorophyll trends are not significant anywhere, with sensitivity roughly 90% of the observed trends in the coastal upwelling zones of South America. New production (and *f*-ratio, not shown) exhibit a similar mean state to chlorophyll, are inversely correlated with SST and decreased throughout the northern equatorial Pacific, especially in the EPWP, and western Pacific (Figures 3g and 3h). New production trend sensitivity was less than 25% of the total variability, hence the most significant stippling of any variable, except in the western equatorial Pacific. New production weakened significantly over the timeseries at -0.037 mmolC m⁻² day⁻¹ yr⁻¹ at 165°E, -0.081 mmolC m⁻² day⁻¹ yr⁻¹ at 110°W and -0.072 mmolC m⁻² day⁻¹ yr⁻¹ at 125°W. However, there were no statistically significant new production trends in the CP and cold tongue. Δ*p*CO₂ is largest in the EP and decreases toward the west (Figure 3i). Overall, the equatorial Pacific basin surface ocean accumulated carbon at 1.85 μatm yr⁻¹ between 2000 and 2020 (*p*CO₂ from the Landschützer product, not shown). Δ*p*CO₂ increased throughout the EP, fastest in the cold tongue at 1–1.5 μatm yr⁻¹. However, the Δ*p*CO₂ basin

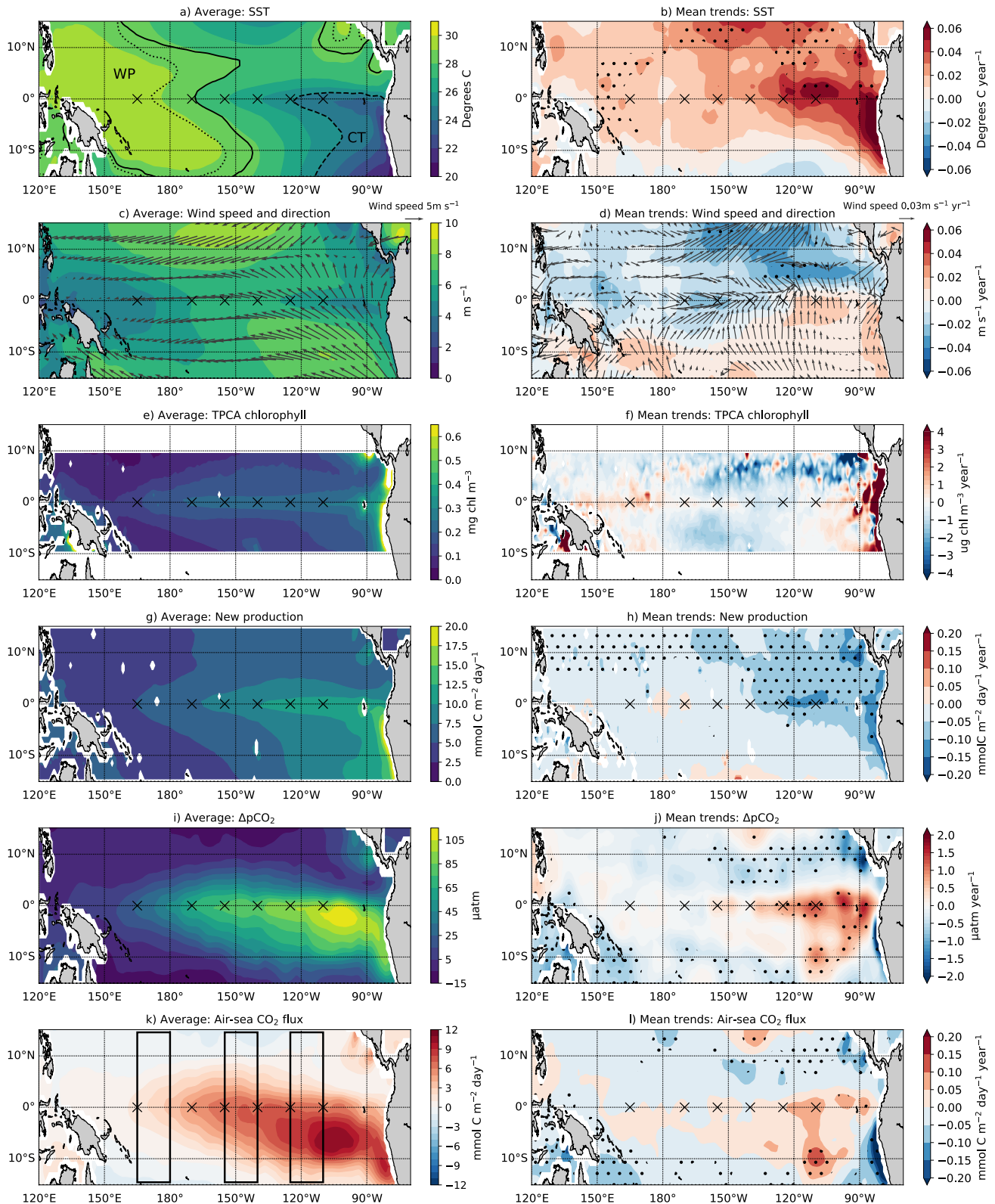


Figure 3.

average trend was $-0.167 \mu\text{atm yr}^{-1}$, meaning that $p\text{CO}_2$ increased more slowly in the ocean than the atmosphere, due to $p\text{CO}_2$ decreases in the EPWP and west of 140°W (Figure 3j). Air-sea CO_2 flux is largest throughout the cold tongue with a maximum at around 110°W , 10°S increasing at $45 \text{ mmolC m}^{-2} \text{ yr}^{-1}$ (Figure 3k). Weaker outgassing occurs west of the dateline and away from the equator in a horse shoe shape, with a minimum at 140°W , 15°N . Air-sea CO_2 flux increased most rapidly at 110°W 10°S in the east Pacific cold tongue (Figure 3l), but weakened everywhere off the equator, especially north of the equator in the EPWP and in the central and western Pacific. Trends are significant in the southern region of the cold tongue and north of the equator. At the moorings, air-sea CO_2 flux weakened by $-0.038 \text{ mmolC m}^{-2} \text{ day}^{-1} \text{ yr}^{-1}$ at 165°E and increased by $0.073 \text{ mmolC m}^{-2} \text{ day}^{-1} \text{ yr}^{-1}$ at 110°W and $0.049 \text{ mmolC m}^{-2} \text{ day}^{-1} \text{ yr}^{-1}$ at 125°W but not significantly in the CP.

3.4. Interannual Variability Anomalies

To characterize interannual variability, we individually composite the three ENSO phases (La Niña, EP and CP El Niño) and subtract the neutral state to get anomaly maps (Figure 4).

SST is warmest during EP El Niño (Figure 4a) and coolest during La Niña (Figure 4c). The EPWP and WPWP bounding isotherms join during EP events, and the WPWP extent reaches its minimum during La Niña. The cold tongue is almost non-existent during EP events and reaches its maximum extent during La Niña. CP events generate the strongest SST gradient across the Pacific, with large decreases in the spatial extent of the cold tongue (Figure 4b). During CP events, the WPWP and cold tongue are similar to mean conditions (Figure 3a). Wind speeds strengthened and reach their highest values at 170°W during La Niña (Figure 4f). During EP El Niño, the winds reverse and are weaker in the central and western Pacific, but increase slightly in the cold tongue (Figure 4d). CP events increase wind speeds in the cold tongue, and decrease winds in the EPWP and WPWP. There is a substantial wind speed anomaly gradient during CP events between the northern and southern equatorial Pacific, particularly in the central and west which are dominated by south to south-westerly wind anomalies (Figure 4e).

Chlorophyll is highest during La Niña (Figure 4i) and lowest during El Niño (Figure 4g), and the largest increases for both EP and La Niña events are in the far western Pacific at 165°E . CP events are most similar to neutral conditions, but chlorophyll increases slightly throughout the eastern and CP, and decreases in the western Pacific between the dateline and 165°E (Figure 4h). New production anomalies during EP and La Niña are similar to chlorophyll and inverse to SST (Figures 4j and 4l). Chlorophyll during CP events exhibits the smallest change of any ENSO phase but there is a strong east-west gradient and also north-south over the equator (Figure 4k).

$\Delta p\text{CO}_2$ decreases across the Pacific during EP, particularly in the cold tongue (Figure 4m) and increases during La Niña, especially in the western Pacific (Figure 4o). CP events have the weakest $\Delta p\text{CO}_2$ change with a slight increase in the cold tongue but generally decrease everywhere (Figure 4n). Air-sea CO_2 flux is depressed during EP across the Pacific (Figure 4p) and amplified during La Niña, particularly west of 140°W , with slight decreases in the cold tongue (Figure 4r). The largest CO_2 flux variability between events is in the central and western Pacific between 140°W and the dateline (Figures 4p–4r). CP events have the smallest magnitude change of outgassing, however the strongest gradient between the east and west (Figure 4q). CP events amplify outgassing in the cold tongue, the most of any phase, and decrease outgassing west of 140°W , in the WPWP and the EPWP. CP events drive the weakest CO_2 source conditions of any phase at 165°E , and lead to near sink conditions (Figure 4q).

3.5. Correlation Analysis

A lagged cross-correlation analysis between the air-sea CO_2 flux and new production showed the maximum correlation occurred when new production lagged the air-sea CO_2 flux by 1 month. Such a lag relationship was most apparent in the EP. However, the improvement in correlation at 1 month lag compared to no lag was extremely small. For example, in the east, r^2 increased from 0.974 to 0.980 and the average r^2 increase across the

Figure 3. The average (left column) and mean rolling trend (60 rolling, 17 years trends starting between 1998–01 and 2002–12 and ending between 2015–01 and 2019–12; right column, stippling indicates significant trends) for seven biological and physical variables. Black crosses are the location of the equatorial TAO/TRITON moorings and the data at these pixels for new production and CO_2 flux are identical to that used in Figure 2. (a and b) Reynolds et al. (2002) OISST, the dotted black contour in panel (a) is the 28.5°C contour defining the east and western warm pool (annotated WP) for 1997–2002 and the solid black is for 2015–2020. The dashed line is the 25°C cold tongue isotherm (annotated CT) (c and d) Cross-Calibrated Multi-Platform surface wind speed and direction, (e and f) Tropical Pacific Chlorophyll Algorithm chlorophyll, (g and h) L2011a new production, (i and j) Landschützer $\Delta p\text{CO}_2$, and (k and l) Landschützer air-sea CO_2 flux. The black rectangular boxes in panel (k) are the 15°N – 15°S 165°E – 180°W western box, 155° – 150°W central box and 125° – 110°W eastern box referred to in Table 1.

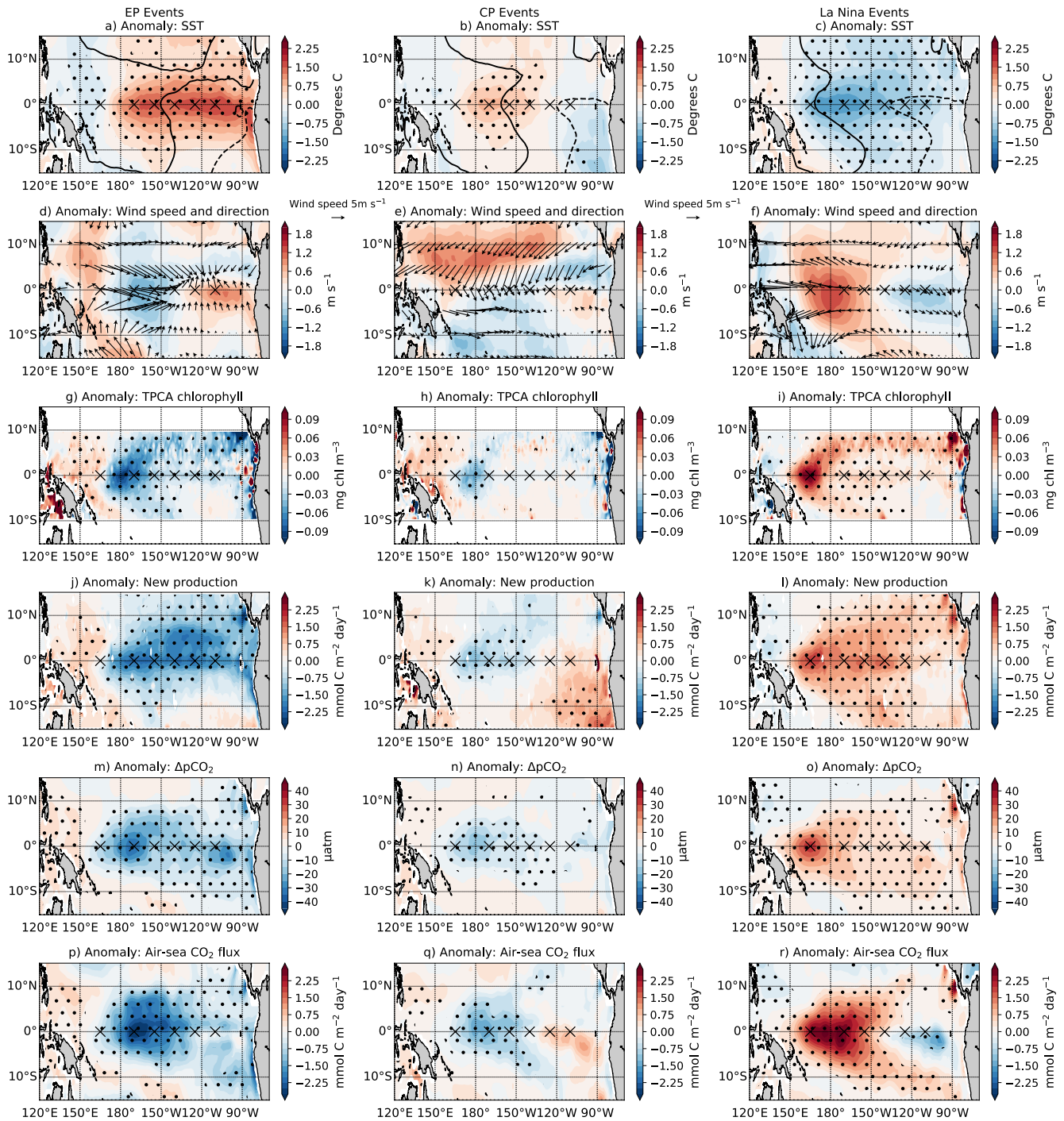


Figure 4. Spatial maps for eastern Pacific (EP; left), central Pacific (CP; middle), and La Niña (right) anomalies (El Niño–Southern Oscillation [ENSO] phase minus neutral conditions; red indicates a positive anomaly) for (a–c) Reynolds et al. (2002) sea surface temperature; solid line indicates the 28.5°C warm pool isotherm and the dashed line is the 25°C cold tongue isotherm, (d–f) Cross-Calibrated Multi-Platform surface wind speed and direction, (g–i) Tropical Pacific Chlorophyll Algorithm chlorophyll, (j–l) L2011a new production, (m–o) Landschützer $\Delta p\text{CO}_2$, and (p–r) Landschützer air-sea CO_2 flux. CP El Niño conditions are periods of EMI ≥ 0.5 . ENSO conditions are periods where the Multivariate ENSO Index v2 exceeds ± 0.5 , and for EP events, do not overlap with CP months. Black stippling indicates regions of significant difference ($p < 0.05$) for that variable between neutral and each ENSO condition.

basin was 0.0007. Thus, we consider this lag difference the air-sea CO_2 flux and new production to be negligible. The correlation at zero lag between air-sea CO_2 flux and new production is lowest in the western Pacific (0.845) compared with the central (0.973) and east (0.974). Thus, air-sea CO_2 flux and new production variability are

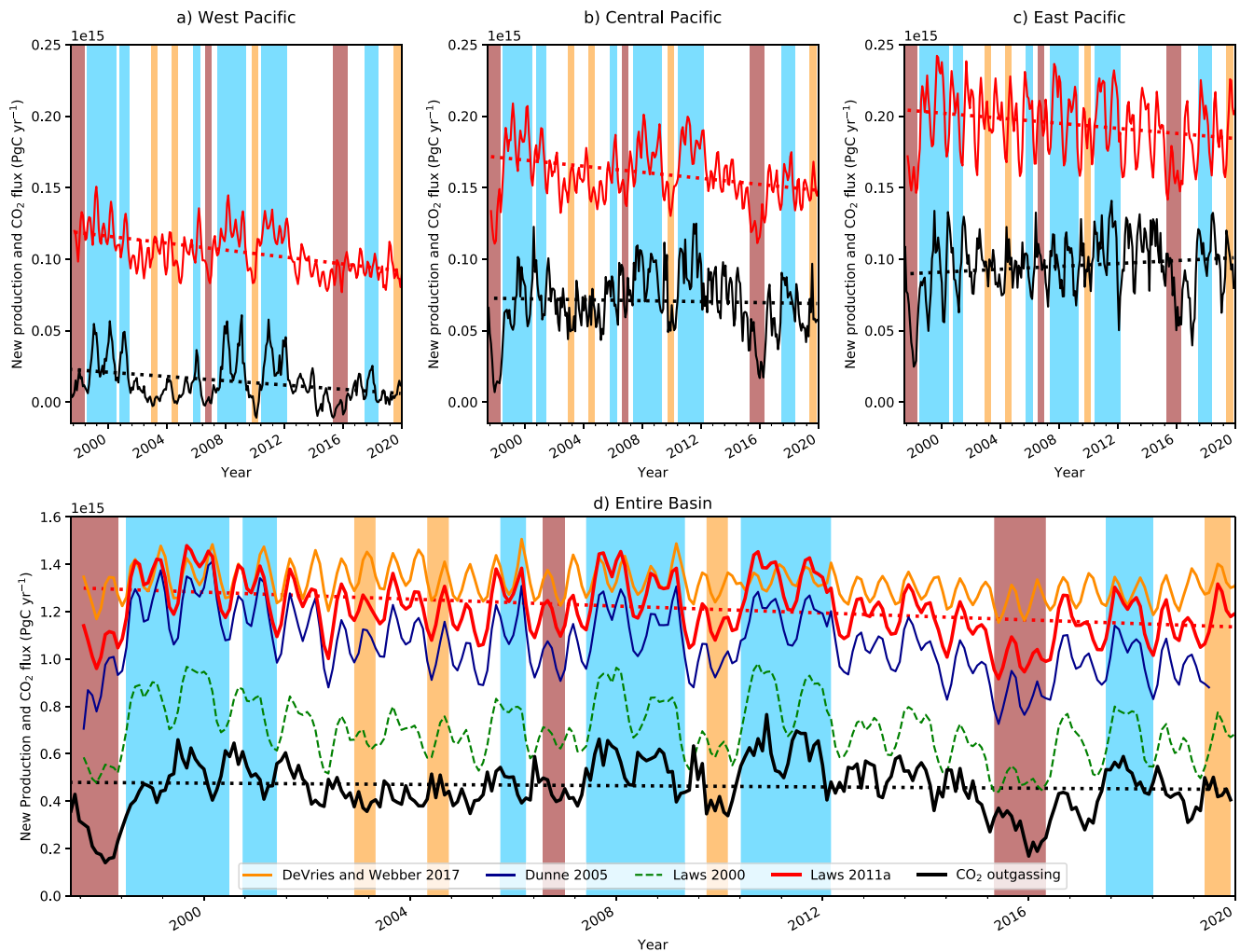


Figure 5. Air-sea CO_2 flux and new production area integrations in PgC yr^{-1} from 15°N to 15°S , for (a) western (165°E – 180°), (b) central (155° – 140°W), (c) eastern (125° – 110°W), and (d) entire tropical Pacific basin (150°E – 90°W). Red line is new production and black line is the air-sea CO_2 flux. Dashed lines indicate the 2000–2020 trends. Statistics are provided in Table 1. Three additional new production models—SIMPLE-TRIM climatology from DeVries and Weber (2017; orange), Dunne et al. (2005; blue), and Laws et al. (2000; dashed green)—are included for comparison in the basin-wide estimates. Vertical shaded bars indicate eastern Pacific El Niño (red), central Pacific El Niño (orange), and La Niña (blue) events.

generally highly correlated. The relationship is slightly different depending on ENSO, for example, the lowest correlation occurs in the CP during CP events (not shown). A linearly detrended time-series correlation (not shown) is almost identical to the 2000–2020 spatial patterns, indicating that correlation variability is not due to the decadal trend but due to seasonal and interannual variability.

3.6. Basin-Scale Averaged Decadal Trends

Decadal trends (2000–2020) show that both new production and air-sea CO_2 flux have decreased across the basin (Table 1, Figure 5d). The declines in new production and air-sea CO_2 fluxes are greatest in the west and CP with a small CO_2 flux increase in the EP (Figures 5a–5c). The CO_2 flux trend in the EP is not significant, primarily due to large increases in the EPWP countering the changes in the equatorial cold tongue (Figures 3l and 5c). The CO_2 flux 60 months mean rolling trends are relatively robust, only biased by a few outlier month combinations evidenced by the difference between mean and median p -values in Table 1 which are significant or close to significant except in the west. New production is always larger, and is declining faster than the rate of air-sea CO_2 flux (Table 1). The result of this is that the difference between CO_2 flux and new production is declining throughout the whole basin with the greatest decline in the EP (Figures 5c and 5d). The ENSO percentage differences show

that across the basin, EP depresses new production, La Niña increases new production and CP has little influence (Table 1). In comparison, EP events decrease CO₂ flux more than new production, La Niña increases CO₂ flux more than new production, and CP events decrease CO₂ flux slightly, primarily in the western Pacific which drove this region to a carbon sink during 2010 (Figure 5a, Table 1). In comparison, EP events drive the eastern and CP to their weakest source conditions (Figures 5b and 5c).

For the 15°N–15°S region used throughout this analysis, the new production mean was 1.213 ± 0.121 PgC yr⁻¹ and CO₂ flux mean was 0.459 ± 0.109 PgC yr⁻¹ (Table 1). The basin-wide mean L2011a new production was within the range of the 1.193 ± 0.113 PgC yr⁻¹ mean and standard deviation of the three similar new production models; L2011a, Dunne et al. (2005) and DeVries and Weber (2017) (Figure 5d). To compare with previous estimates, we also computed regional carbon fluxes. For 10°N–10°S and 180°–90°W, new production was 0.716 ± 0.092 PgC yr⁻¹, slightly lower than the 0.85 PgC yr⁻¹ from F. P. Chavez and Barber (1987) and air-sea CO₂ flux was 0.412 ± 0.097 PgC yr⁻¹. The difference between the 10°N–10°S and 15°N–15°S regions are quite large, particularly for new production. For 1°N–1°S and 135°E–90°W box (Le Borgne, Feely, & Mackey, 2002) air-sea CO₂ flux was 0.062 ± 0.017 PgC yr⁻¹ and new production was 0.115 ± 0.018 PgC yr⁻¹, which was between the upper (0.134 PgC yr⁻¹) and lower (0.106 PgC yr⁻¹) estimates of Le Borgne, Feely, and Mackey (2002) for 1980–2000. For 180°–90°W and 5°N–5°S Wyrтки (1981) box used by Chavez et al. (1996) who calculated 0.65–0.98 PgC yr⁻¹, we calculated new production to be 0.40 ± 0.063 PgC yr⁻¹, roughly 61% of their lower estimates and air-sea CO₂ flux to be 0.25 ± 0.066 PgC yr⁻¹.

4. Discussion

4.1. Physical Drivers of Decadal Trends in New Production and CO₂ Flux

Here, we show how spatial changes in air-sea CO₂ flux and new production are primarily driven by changes in wind speed, wind divergence driven upwelling, SST and ENSO phase.

In the EP (15°N–15°S, East of 140°W), over the mean rolling trend (1998–2002 to 2015–2019) period, increased wind speeds in the cold tongue (Figure 3d) have enhanced upwelling and decreased SST (England et al., 2014; Seager et al., 2019). The cold tongue has experienced weakly increasing southerly winds, likely driving upwelling there (Figure 3d). North of the equator, wind speeds have decreased and thus wind direction change is towards southerlies and more convergent compared to mean conditions. Enhanced upwelling of cool water in the cold tongue increases the availability of nutrients and DIC at the surface, and has resulted in *p*CO₂ increasing faster in the EP than in the atmosphere (Figure 3i; Sutton, Feely, et al., 2014). In addition to driving upwelling, wind speed increases have also enhanced gas transfer, and combined with increased *p*CO₂, have driven increased CO₂ outgassing in the cold tongue. In the EPWP region north of the equator there were large decreases in Δp CO₂, wind speed and thus CO₂ flux (Table 1, Figures 3d, 3j and 3l; England et al., 2014). Increasing SSTs in the EPWP (Figure 3b) decrease the solubility of CO₂, which increases Δp CO₂ and CO₂ flux (Raven & Falkowski, 1999; Weiss, 1974). Therefore other drivers such as wind speed, which is influenced by coastal geometry (Pennington et al., 2006), are causing the hemispheric asymmetry in CO₂ outgassing trends north and south of the equator in the EP (Figure 3i). Precipitation related surface freshening may also play a minor role in reducing Δp CO₂ through dilution of DIC and alkalinity (Ho & Schanze, 2020; Turk et al., 2010). New production decreased significantly and most rapidly in the EPWP due to the same factors as CO₂ flux, but did not significantly change in the cold tongue (Figure 3h). The *f*-ratio formulation has an inverse relationship with SST (Henson et al., 2011; Laws et al., 2011), so warming was a major factor in decreasing new production in the EPWP. Chlorophyll, another proxy for primary productivity, increased slightly but not significantly in the cold tongue (Figures 3b, 3f and 3h). Iron limitation (Behrenfeld et al., 1996, 2005; Coale et al., 1996; Landry et al., 1997; Minas et al., 1986; Strutton et al., 2011), and also silicate limitation (Dugdale et al., 2011) is likely the key reason for no change in the biological uptake of carbon despite rising DIC and CO₂ outgassing in the cold tongue. In general, the trends are robust in the cold tongue as trend sensitivity here is around 50% of the observed trends. The combined effect of the trends in new production, Δp CO₂, SST and wind speed, is that the cold tongue increased outgassing is offset by reduced outgassing in the EPWP and produces a weak positive trend in the EP air-sea CO₂ flux, and decreased new production (Figures 3 and 5c, Table 1).

The oligotrophic central and western Pacific, west of 140°W, has become a weaker CO₂ source since 2000 (Figure 3l) and can infrequently become a carbon sink (Figures 2 and 5a; F. Chavez et al., 1999; Hauck

et al., 2020; Sutton, Feely, et al., 2014). Sink events do not clearly overlap with any particular ENSO phase (Figure 2), but CP events cause the weakest CO₂ source conditions (Figure 4q). New production is around 7 times larger than CO₂ flux in the west, compared to ~2 times larger in the east, higher than previous estimates (Table 1; Cosca, 2003; Feely et al., 2002; Lefèvre et al., 1994; Quay, 1997). CO₂ flux in the western Pacific has decreased at a faster rate (−3.4% yr^{−2}) than new production (−0.9% yr^{−2}) for the mean rolling trends between 1998 and 2020 (Table 1) due to the following three key factors: wind speed decreases, warm pool freshening and expansion, and changing ENSO patterns. First, wind speed has decreased in the central and western Pacific (Figure 3d; Yasunaka et al., 2019), and ocean pCO₂ increased more slowly in the western Pacific than in the atmosphere, causing decreased outgassing (Figure 4o, Sutton, Feely, et al., 2014). Second, the >28.5°C WPWP is growing larger, warmer and fresher due to anthropogenic climate change (Figure 4a; Cravatte et al., 2009; Weller et al., 2016). New production has decreased due to increasing SSTs because of the inverse SST to *f*-ratio formulation (Figures 2, 3b and 3h; Laws et al., 2011). CO₂ flux is decreasing despite warmer SSTs causing lower solubility and higher pCO₂. Third, the western Pacific experiences the largest and most widespread ENSO anomalies (Figure 4), and CP events have a similar east-west gradient as seen for the 20-year trends. The CP (140°–160°W) is a region of large interannual variability, because it is a transitional zone between the cold tongue and WPWP, which migrates depending on season and ENSO phase (Figures 4a–4c; Delcroix & McPhaden, 2002; Maes et al., 2004; Turk et al., 2001; Weller et al., 2016). In comparison to a longer comparison period such as 1981–2015, our 17 years mean rolling trends for CO₂ flux and wind speed are more similar than SST and pCO₂ which show distinct differences across the basin (Figure 3, right column; Yasunaka et al., 2019, Figure 12). These differences are likely due to cool and warm phases of Pacific Decadal Variability. Our analysis period 1998–2020 was dominated by “cool phase” conditions, with 6 La Niña events and largely cool periods of Pacific Decadal Variability depressing equatorial Pacific SST during the early 21st century (England et al., 2014; McPhaden & Zhang, 2004; Meehl et al., 2021; Power et al., 2021). The shift from cool to warm Pacific Decadal Variability around 2015 may have further influenced the CP like trends presented (Figure 3 right column and Figure 4, center column). Therefore, as CP and La Niña events are becoming more frequent (Cai, Santoso, et al., 2015; Cai, Wang, et al., 2015; Freund et al., 2019), they could be causing or amplifying the decadal trends in the carbon budget, as explained in detail below.

4.2. ENSO Influence on CO₂ Flux and New Production

CO₂ outgassing and new production are strongly influenced by ENSO conditions (Table 1; Figures 2, 4 and 5). ENSO is changing character over time, toward less frequent but more intense EP events and more common CP and La Niña events (Cai, Santoso, et al., 2015; Cai, Wang, et al., 2015; Freund et al., 2019; T. Lee & McPhaden, 2010; Yeh et al., 2009). More frequent CP events are likely to drive the EP toward a stronger CO₂ source, and the western Pacific into a weak source or an occasional sink, either causing, or at least amplifying the 20-year trends. Compared to EP El Niño events, CP events are similar to neutral conditions (Table 1; Gierach et al., 2012), but cause steep east-west gradients in all variables (Figure 4, center column). West of the dateline and specifically around 165°E, past the maximum extent of EP events (~170°W; Figure 4p), all variables except wind speed reach their most neutral values during CP events (Figure 4, center column; Table 1; Messié & Chavez, 2013). CP events drive a strong chlorophyll decrease in the central and western Pacific and have been linked to a deeper thermocline, reduced surface nitrate and pCO₂, and barrier layer thickening (Gierach et al., 2012; Messié & Chavez, 2013; Radenac et al., 2012; Turk et al., 2011). These factors drive weak sink periods in the western Pacific during CP events, stronger than the very brief EP event sink periods at 155°E (F. Chavez et al., 1999). At the basin scale, the weak western Pacific sink during CP El Niño is balanced by CO₂ flux increases in the EP, where the largest outgassing of any ENSO phase is seen between 135°W and 100°W, resulting in no significant basin-wide changes compared with neutral conditions (Figure 4q; Table 1).

EP events reduce outgassing in the eastern and CP due to weakened trade winds and increased SSTs, which result in reduced gas transfer velocity, flattening of the thermocline, and increased stratification (Figures 4a and 4d; F. Chavez et al., 1999; Feely et al., 2002; Ishii et al., 2014; Sutton, Feely, et al., 2014; Yasunaka et al., 2019). EP events reduce outgassing twice as much as they decrease new production (Table 1). Thus, air-sea CO₂ flux has a larger impact than new production on the variability of surface ΔpCO₂ and the carbon budget at interannual scales, despite new production being larger overall.

La Niña onset and peak enhances wind speed, upwelling, and decreases SST, predominantly west of 140°W (Figures 4c and 4i; F. Chavez et al., 1999; Larkin & Harrison, 2002). Interestingly, weaker winds are observed in the cold tongue region (Figure 4c), possibly due to divergent zonal wind anomalies, or because wind speed increases occur here before the onset and after maturity of La Niña events (Ryan et al., 2002). The result is that CO₂ flux in the cold tongue is slightly weaker than neutral conditions, but this decrease is small compared to the overall increase throughout the basin. The largest changes of any event occur in the western Pacific where new production and air-sea CO₂ flux are enhanced to their largest values (Figures 4l and 4r). More frequent La Niña events (Cai, Wang, et al., 2015) will strengthen both outgassing and new production (Figures 4l, and 4r), however CP patterns align more closely with the 20-year trends as they are typically closer to the mean state compared to La Niña events (Figures 3h, 3l, 4k and 4q).

In summary, one of the reasons the cold tongue is becoming a stronger source of carbon to the atmosphere is because La Niña and particularly CP events are becoming more frequent and EP events are become less frequent but more intense. The western Pacific is becoming a weaker source during CP events and over time, but there is intense outgassing there during La Niña events.

4.3. Observational Improvements Necessary to Close the Carbon Budget

Upwelled DIC can be either degassed to the atmosphere, exported to depth as biogenic particles or advected meridionally or zonally (Falkowski et al., 2003; Liao et al., 2020; Sabine et al., 2004). A lack of accurate horizontal advection, Ekman transport and even in situ export flux data impedes our ability to close the carbon budget in this analysis. We use new production as a proxy for export flux and show that it is not highly sensitive to the *f*-ratio parameterization selected (Figures 1d and 5d). The L2011a, Dunne et al. (2005) and SIMPLE-TRIM models provide similar estimates of new production. However, new production estimates used here likely overestimate the sinking POC flux due to advection away from the equator through Ekman transport (Liao et al., 2020). Lateral advection has been measured to be roughly equivalent or slightly larger than new production (Landry et al., 1997), and has been shown to be a larger component of the equatorial Pacific carbon budget during EP events than was previously thought (Liao et al., 2020). Accurately quantifying the export flux could help to accurately derive the lateral flux as a residual. Future work should include more in situ POC export flux and new production observations to validate models, and work toward community accepted new and export production models. This would permit closure of the carbon budget through remote sensing, modeling and interpolation methods.

5. Conclusions

Our study investigates the interannual to decadal variability in tropical Pacific new production and air-sea CO₂ flux and their relationships to other environmental variables. The response of new production and air-sea CO₂ flux to interannual physical variability is consistent across the three ENSO phases. However, for the mean rolling trends over the 1998–2020 period, new production and air-sea CO₂ flux show a different behavior. In the cold tongue, increases in air-sea CO₂ flux outgassing are associated with increased upwelling but neither chlorophyll nor new production significantly change, perhaps due to iron and silicate limitation. Outside the cold tongue region, both new production and CO₂ fluxes generally declined, however the CO₂ flux rate decreased at a much slower rate than new production. In the western Pacific, Ocean *p*CO₂ is increasing more slowly than the atmosphere (Sutton, Feely, et al., 2014), and forces 165°E to an occasional CO₂ sink during strong El Niños, particularly CP events. The divergent behavior in new production and CO₂ fluxes suggest they are responding differently to Pacific Decadal Variability (Meehl et al., 2021; Power et al., 2021) and perhaps climate change.

To clearly elucidate the processes driving new production and air-sea CO₂ flux variability requires a carbon budget approach which is not possible with existing observations. The largest uncertainty to closing the budget is the role of horizontal advection of DIC and nutrients (Landry et al., 1997; Le Borgne, Barber, et al., 2002, Le Borgne, Feely, & Mackey, 2002; Murray et al., 1994). Coupled physical and biogeochemical models, preferably with data assimilation, provide a way to close the carbon budget and produce the insight required to understand how new production and air-sea CO₂ fluxes will respond to future climate variability and change.

Conflict of Interest

The authors declare no conflicts of interest relevant to this study.

Data Availability Statement

Python 3.7 was used here for analysis, with packages including xarray, Numpy, Scipy, Pandas, and Matplotlib. The source code can be found at <https://doi.org/10.5281/zenodo.5120943>.

Acknowledgments

N. A. Pittman and P. G. Strutton acknowledge support from the ARC Centre of Excellence for Climate Extremes (CE170100023). This research was undertaken with the assistance of resources and services from the National Computational Infrastructure (NCI), which is supported by the Australian Government. The authors would like to thank the NASA/Goddard Space Flight Center for freely providing satellite euphotic depth data for SeaWiFS and MODIS-Aqua and all other data providers described in the methods for making their data openly accessible. This manuscript is PMEL contribution number 5263. Open access publishing facilitated by University of Tasmania, as part of the Wiley - University of Tasmania agreement via the Council of Australian University Librarians.

References

- Ashok, K., Behera, S. K., Rao, S. A., Weng, H., & Yamagata, T. (2007). El Niño Modoki and its possible teleconnection. *Journal of Geophysical Research*, *112*(C11). <https://doi.org/10.1029/2006JC003798>
- Aufdenkampe, A. K., McCarthy, J. J., Navarette, C., Rodier, M., Dunne, J., & Murray, J. W. (2002). Biogeochemical controls on new production in the tropical Pacific. *Deep Sea Research Part II: Topical Studies in Oceanography*, *49*(13–14), 2619–2648. [https://doi.org/10.1016/S0967-0645\(02\)00051-6](https://doi.org/10.1016/S0967-0645(02)00051-6)
- Aufdenkampe, A. K., McCarthy, J. J., Rodier, M., Navarette, C., Dunne, J., & Murray, J. W. (2001). Estimation of new production in the tropical Pacific. *Global Biogeochemical Cycles*, *15*(1), 101–112. <https://doi.org/10.1029/2000GB001268>
- Behrenfeld, M. J., Bale, A. J., Kolber, Z. S., Aiken, J., & Falkowski, P. G. (1996). Confirmation of iron limitation of phytoplankton photosynthesis in the equatorial Pacific Ocean. *Nature*, *383*(6600), 508. <https://doi.org/10.1038/383508a0>
- Behrenfeld, M. J., Boss, E., Siegel, D. A., & Shea, D. M. (2005). Carbon-based ocean productivity and phytoplankton physiology from space. *Global Biogeochemical Cycles*, *19*(1). <https://doi.org/10.1029/2004GB002299>
- Bennington, V., McKinley, G. A., Dutkiewicz, S., & Ullman, D. (2009). What does chlorophyll variability tell us about export and air-sea CO₂ flux variability in the North Atlantic? *Global Biogeochemical Cycles*, *23*(3). <https://doi.org/10.1029/2008GB003241>
- Bisson, K., Siegel, D. A., & DeVries, T. (2020). Diagnosing mechanisms of ocean carbon export in a satellite-based food web model. *Frontiers in Marine Science*, *7*, 505. <https://doi.org/10.3389/fmars.2020.00505>
- Bisson, K. M., Siegel, D. A., DeVries, T., Cael, B. B., & Buesseler, K. O. (2018). How data set characteristics influence ocean carbon export models. *Global Biogeochemical Cycles*, *32*(9), 1312–1328. <https://doi.org/10.1029/2018GB005934>
- Cai, W., Santoso, A., Wang, G., Yeh, S. W., An, S. I., Cobb, K. M., et al. (2015). ENSO and greenhouse warming. *Nature Climate Change*, *5*(9), 849–859. <https://doi.org/10.1038/nclimate2743>
- Cai, W., Wang, G., Santoso, A., McPhaden, M. J., Wu, L., Jin, F. F., et al. (2015). Increased frequency of extreme La Niña events under greenhouse warming. *Nature Climate Change*, *5*(2), 132–137. <https://doi.org/10.1038/nclimate2492>
- Chavez, F., Strutton, P., Friederich, G., Feely, R., Feldman, G., Foley, D., & McPhaden, M. (1999). Biological and chemical response of the equatorial Pacific Ocean to the 1997–98 El Niño. *Science*, *286*(5447), 2126–2131. <https://doi.org/10.1126/science.286.5447.2126>
- Chavez, F. P., & Barber, R. T. (1987). An estimate of new production in the equatorial Pacific. *Deep-Sea Research Part A. Oceanographic Research Papers*, *34*(7), 1229–1243. [https://doi.org/10.1016/0198-0149\(87\)90073-2](https://doi.org/10.1016/0198-0149(87)90073-2)
- Chavez, F. P., Buck, K. R., Service, S. K., Newton, J., & Barber, R. T. (1996). Phytoplankton variability in the central and eastern tropical Pacific. *Deep Sea Research Part II: Topical Studies in Oceanography*, *43*(4–6), 835–870. [https://doi.org/10.1016/0967-0645\(96\)00028-8](https://doi.org/10.1016/0967-0645(96)00028-8)
- Chavez, F. P., Strutton, P. G., & McPhaden, M. J. (1998). Biological-physical coupling in the central equatorial Pacific during the onset of the 1997–98 El Niño. *Geophysical Research Letters*, *25*(19), 3543–3546. <https://doi.org/10.1029/98GL02729>
- Chiodi, A. M., Dunne, J. P., & Harrison, D. E. (2019). Estimating air-sea carbon flux uncertainty over the tropical Pacific: Importance of winds and wind analysis uncertainty. *Global Biogeochemical Cycles*, *33*(3), 370–390. <https://doi.org/10.1029/2018GB006047>
- Coale, K. H., Johnson, K. S., Fitzwater, S. E., Gordon, R. M., Tanner, S., Chavez, F. P., et al. (1996). A massive phytoplankton bloom induced by an ecosystem-scale iron fertilization experiment in the equatorial Pacific Ocean. *Nature*, *383*(6600), 495–501. <https://doi.org/10.1038/383495a0>
- Cosca, E. (2003). Seasonal and interannual CO₂ fluxes for the central and eastern equatorial Pacific Ocean as determined from fCO₂-SST relationships. *Journal of Geophysical Research*, *108*(C8), 3278. <https://doi.org/10.1029/2000JC000677>
- Cravatte, S., Delcroix, T., Zhang, D., McPhaden, M., & Leloup, J. (2009). Observed freshening and warming of the western Pacific warm pool. *Climate Dynamics*, *33*(4), 565–589. <https://doi.org/10.1007/s00382-009-0526-7>
- Delcroix, T., & McPhaden, M. (2002). Interannual sea surface salinity and temperature changes in the western Pacific warm pool during 1992–2000: SSS and SST changes in the western Pacific warm pool. *Journal of Geophysical Research*, *107*(C12), SRF3-1–SRF3-17. <https://doi.org/10.1029/2001JC000862>
- DeVries, T., Primeau, F., & Deutsch, C. (2012). The sequestration efficiency of the biological pump. *Geophysical Research Letters*, *39*(13). <https://doi.org/10.1029/2012GL051963>
- DeVries, T., & Weber, T. (2017). The export and fate of organic matter in the ocean: New constraints from combining satellite and oceanographic tracer observations: Export and fate of marine organic matter. *Global Biogeochemical Cycles*, *31*(3), 535–555. <https://doi.org/10.1002/2016GB005551>
- Dugdale, R., Chai, F., Feely, R., Measures, C., Parker, A., & Wilkerson, F. (2011). The regulation of equatorial Pacific new production and pCO₂ by silicate-limited diatoms. *Deep Sea Research Part II: Topical Studies in Oceanography*, *58*, 477–492. <https://doi.org/10.1016/j.dsr2.2010.08.008>
- Dugdale, R., & Goering, J. (1967). Uptake of new and regenerated forms of nitrogen in primary productivity. *Limnology & Oceanography*, *12*(2), 196–206. <https://doi.org/10.4319/lo.1967.12.2.0196>
- Dunne, J. P., Armstrong, R. A., Gnanadesikan, A., & Sarmiento, J. L. (2005). Empirical and mechanistic models for the particle export ratio. *Global Biogeochemical Cycles*, *19*(4). <https://doi.org/10.1029/2004GB002390>
- Dunne, J. P., Sarmiento, J. L., & Gnanadesikan, A. (2007). A synthesis of global particle export from the surface ocean and cycling through the ocean interior and on the seafloor. *Global Biogeochemical Cycles*, *21*(4). <https://doi.org/10.1029/2006GB002907>
- England, M. H., McGregor, S., Spence, P., Meehl, G. A., Timmermann, A., Cai, W., et al. (2014). Recent intensification of wind-driven circulation in the Pacific and the ongoing warming hiatus. *Nature Climate Change*, *4*(3), 222–227. <https://doi.org/10.1038/nclimate2106>
- Eppley, R. W. (1972). Temperature and phytoplankton growth in the sea. *Fishery Bulletin*, *70*(4), 1063–1085.

- Eppley, R. W., & Peterson, B. J. (1979). Particulate organic matter flux and planktonic new production in the deep ocean. *Nature*, 282(5740), 677–680. <https://doi.org/10.1038/282677a0>
- Falkowski, P. G., Laws, E. A., Barber, R. T., & Murray, J. W. (2003). Phytoplankton and their role in primary, new, and export production. In M. J. R. Fasham (Ed.), *Ocean Biogeochemistry* (pp. 99–121). Springer Berlin Heidelberg. https://doi.org/10.1007/978-3-642-55844-3_5
- Feely, R. A., Boutin, J., Cosca, C. E., Dandonneau, Y., Etcheto, J., Inoue, H. Y., et al. (2002). Seasonal and interannual variability of CO₂ in the equatorial Pacific. *Deep Sea Research Part II: Topical Studies in Oceanography*, 49(13–14), 2443–2469. [https://doi.org/10.1016/S0967-0645\(02\)00044-9](https://doi.org/10.1016/S0967-0645(02)00044-9)
- Feely, R. A., Takahashi, T., Wanninkhof, R., McPhaden, M. J., Cosca, C. E., Sutherland, S. C., & Carr, M. E. (2006). Decadal variability of the air-sea CO₂ fluxes in the equatorial Pacific Ocean. *Journal of Geophysical Research*, 111(C8). <https://doi.org/10.1029/2005JC003129>
- Fiedler, P. C., & Talley, L. D. (2006). Hydrography of the eastern tropical Pacific: A review. *Progress in Oceanography*, 69(2–4), 143–180. <https://doi.org/10.1016/j.pocean.2006.03.008>
- Freund, M. B., Henley, B. J., Karoly, D. J., McGregor, H. V., Abram, N. J., & Dommenget, D. (2019). Higher frequency of central Pacific El Niño events in recent decades relative to past centuries. *Nature Geoscience*, 12(6), 450–455. <https://doi.org/10.1038/s41561-019-0353-3>
- Gierach, M. M., Lee, T., Turk, D., & McPhaden, M. J. (2012). Biological response to the 1997–98 and 2009–10 El Niño events in the equatorial Pacific Ocean. *Geophysical Research Letters*, 39(10). <https://doi.org/10.1029/2012GL051103>
- Hauck, J., Zeising, M., Le Quéré, C., Gruber, N., Bakker, D. C. E., Bopp, L., et al. (2020). Consistency and challenges in the ocean carbon sink estimate for the global carbon budget. *Frontiers in Marine Science*, 7, 571720. <https://doi.org/10.3389/fmars.2020.571720>
- Henson, S. A., Sanders, R., Madsen, E., Morris, P. J., Le Moigne, F., & Quartly, G. D. (2011). A reduced estimate of the strength of the ocean's biological carbon pump. *Geophysical Research Letters*, 38(4). <https://doi.org/10.1029/2011GL046735>
- Henson, S. A., Sarmiento, J. L., Dunne, J. P., Bopp, L., Lima, I. D., Doney, S. C., et al. (2010). Detection of anthropogenic climate change in satellite records of ocean chlorophyll and productivity. *Biogeosciences*, 7, 621–640. <https://doi.org/10.5194/bg-7-621-2010>
- Ho, D. T., & Schanze, J. J. (2020). Precipitation-Induced reduction in surface ocean pCO₂: Observations from the eastern tropical Pacific Ocean. *Geophysical Research Letters*, 47(15). <https://doi.org/10.1029/2020GL088252>
- Iida, Y., Kojima, A., Takatani, Y., Nakano, T., Sugimoto, H., Midorikawa, T., & Ishii, M. (2015). Trends in pCO₂ and sea-air CO₂ flux over the global open oceans for the last two decades. *Journal of Oceanography*, 71(6), 637–661. <https://doi.org/10.1007/s10872-015-0306-4>
- Ishii, M., Feely, R. A., Rodgers, K. B., Park, G. H., Wanninkhof, R., Sasano, D., et al. (2014). Air-sea CO₂ flux in the Pacific Ocean for the period 1990–2009. *Biogeosciences Discussions*, 10(7), 12155–12216. <https://doi.org/10.5194/bgd-10-12155-2013>
- Kahru, M. (2017). Ocean productivity from space: Commentary. *Global Biogeochemical Cycles*, 31(1), 214–216. <https://doi.org/10.1002/2016GB005582>
- Landry, M. R., Barber, R. T., Bidigare, R. R., Chai, F., Coale, K. H., Dam, H. G., et al. (1997). Iron and grazing constraints on primary production in the central equatorial Pacific: An EqPac synthesis. *Limnology & Oceanography*, 42(3), 405–418. <https://doi.org/10.4319/lo.1997.42.3.0405>
- Landschützer, P., Gruber, N., & Bakker, D. (2020). *An Observation-Based Global Monthly Gridded Sea Surface pCO₂ Product From 1982 Onward and Its Monthly Climatology* (NCEI Accession 0160558). Version 5.5. NOAA National Centers for Environmental Information. <https://doi.org/10.7289/V5Z899N6>
- Landschützer, P., Gruber, N., & Bakker, D. C. E. (2016). Decadal variations and trends of the global ocean carbon sink. *Global Biogeochemical Cycles*, 30(10), 1396–1417. <https://doi.org/10.1002/2015GB005359>
- Landschützer, P., Gruber, N., Bakker, D. C. E., & Schuster, U. (2014). Recent variability of the global ocean carbon sink. *Global Biogeochemical Cycles*, 28, 927–949. <https://doi.org/10.1002/2014GB004853>
- Larkin, N. K., & Harrison, D. E. (2002). ENSO warm (El Niño) and cold (La Niña) event life cycles: Ocean surface anomaly patterns, their symmetries, asymmetries, and implications. *Journal of Climate*, 15, 23. [https://doi.org/10.1175/1520-0442\(2002\)015<1118:EWENOAS>2.0.CO;2](https://doi.org/10.1175/1520-0442(2002)015<1118:EWENOAS>2.0.CO;2)
- Laws, E. A., D'Sa, E., & Naik, P. (2011). Simple equations to estimate ratios of new or export production to total production from satellite-derived estimates of sea surface temperature and primary production: Equations for ef ratios. *Limnology and Oceanography: Methods*, 9(12), 593–601. <https://doi.org/10.4319/lom.2011.9.593>
- Laws, E. A., Falkowski, P. G., Smith, W. O., Ducklow, H., & McCarthy, J. J. (2000). Temperature effects on export production in the open ocean. *Global Biogeochemical Cycles*, 14(4), 1231–1246. <https://doi.org/10.1029/1999GB001229>
- Le Borgne, R., Barber, R. T., Delcroix, T., Inoue, H. Y., Mackey, D. J., & Rodier, M. (2002). Pacific warm pool and divergence: Temporal and zonal variations on the equator and their effects on the biological pump. *Deep Sea Research Part II: Topical Studies in Oceanography*, 49(13–14), 2471–2512. [https://doi.org/10.1016/S0967-0645\(02\)00045-0](https://doi.org/10.1016/S0967-0645(02)00045-0)
- Le Borgne, R., Feely, R. A., & Mackey, D. J. (2002). Carbon fluxes in the equatorial Pacific: A synthesis of the JGOFS programme. *Deep Sea Research Part II: Topical Studies in Oceanography*, 49(13–14), 2425–2442. [https://doi.org/10.1016/S0967-0645\(02\)00043-7](https://doi.org/10.1016/S0967-0645(02)00043-7)
- Le Borgne, R., & Rodier, M. (1997). Net zooplankton and the biological pump: A comparison between the oligotrophic and mesotrophic equatorial Pacific. *Deep Sea Research Part II: Topical Studies in Oceanography*, 44(9–10), 2003–2023. [https://doi.org/10.1016/S0967-0645\(97\)00034-9](https://doi.org/10.1016/S0967-0645(97)00034-9)
- Lee, T., & McPhaden, M. J. (2010). Increasing intensity of El Niño in the central-equatorial Pacific. *Geophysical Research Letters*, 37(14). <https://doi.org/10.1029/2010GL044007>
- Lee, Z., Weidemann, A., Kindle, J., Arnone, R., Carder, K. L., & Davis, C. (2007). Euphotic zone depth: Its derivation and implication to ocean-color remote sensing. *Journal of Geophysical Research*, 112(C3), C03009. <https://doi.org/10.1029/2006JC003802>
- Lefèvre, N., Andrié, C., Dandonneau, Y., Reverdin, G., & Rodier, M. (1994). PCO₂, chemical properties, and estimated new production in the equatorial Pacific in January–March 1991. *Journal of Geophysical Research*, 99(C6), 12639. <https://doi.org/10.1029/94JC00293>
- Li, Z., & Cassar, N. (2016). Satellite estimates of net community production based on O₂/Ar observations and comparison to other estimates: Satellite NCP estimates. *Global Biogeochemical Cycles*, 30(5), 735–752. <https://doi.org/10.1002/2015GB005314>
- Liao, E., Resplandy, L., Liu, J., & Bowman, K. W. (2020). Amplification of the ocean carbon sink during El Niños: Role of Poleward Ekman transport and influence on atmospheric CO₂. *Global Biogeochemical Cycles*, 34(9). <https://doi.org/10.1029/2020GB006574>
- Longhurst, A. R. (2007). *Ecological geography of the sea* (Vol. 2). Elsevier.
- Maes, C., Picaut, J., Kuroda, Y., & Ando, K. (2004). Characteristics of the convergence zone at the eastern edge of the Pacific warm pool: Pacific warm pool convergence zone. *Geophysical Research Letters*, 31(11). <https://doi.org/10.1029/2004GL019867>
- Marathe, S., Ashok, K., Swapna, P., & Sabin, T. P. (2015). Revisiting El Niño modokis. *Climate Dynamics*, 45(11–12), 3527–3545. <https://doi.org/10.1007/s00382-015-2555-8>
- McCarthy, J. J., Garside, C., Nevins, J. L., & Barber, R. T. (1996). New production along 140 W in the equatorial Pacific during and following the 1992 El Niño event. *Deep Sea Research Part II: Topical Studies in Oceanography*, 43(4–6), 1065–1093. [https://doi.org/10.1016/0967-0645\(96\)00022-7](https://doi.org/10.1016/0967-0645(96)00022-7)
- McKinley, G. A., Fay, A. R., Lovenduski, N. S., & Pilcher, D. J. (2017). Natural variability and anthropogenic trends in the ocean carbon sink. *Annual Review of Marine Science*, 9(1), 125–150. <https://doi.org/10.1146/annurev-marine-010816-060529>
- McKinley, G. A., Follows, M. J., & Marshall, J. (2004). Mechanisms of air-sea CO₂ flux variability in the equatorial Pacific and the North Atlantic. *Global Biogeochemical Cycles*, 18(2). <https://doi.org/10.1029/2003GB002179>

- McPhaden, M. J., Zebiak, S. E., & Glantz, M. H. (2006). ENSO as an integrating concept in Earth Science. *Science*, *314*(5806), 1740–1745. <https://doi.org/10.1126/science.1132588>
- McPhaden, M. J., & Zhang, D. (2004). Pacific Ocean circulation rebounds. *Geophysical Research Letters*, *31*, L18301. <https://doi.org/10.1029/2004GL020727>
- Meehl, G. A., Hu, A., Castruccio, F., England, M. H., Bates, S. C., Danabasoglu, G., et al. (2021). Atlantic and Pacific tropics connected by mutually interactive decadal-timescale processes. *Nature Geoscience*, *14*, 36–42. <https://doi.org/10.1038/s41561-020-00669-x>
- Messié, M., & Chavez, F. P. (2013). Physical-biological synchrony in the global ocean associated with recent variability in the central and western equatorial Pacific. *Journal of Geophysical Research: Oceans*, *118*(8), 3782–3794. <https://doi.org/10.1002/jgrc.20278>
- Minas, H. J., Minas, M., & Packard, T. T. (1986). Productivity in upwelling areas deduced from hydrographic and chemical fields. *Limnology & Oceanography*, *31*(6), 1182–1206. <https://doi.org/10.4319/lo.1986.31.6.1182>
- Morel, A. (1991). Light and marine photosynthesis: A spectral model with geochemical and climatological implications. *Progress in Oceanography*, *26*(3), 263–306. [https://doi.org/10.1016/0079-6611\(91\)90004-6](https://doi.org/10.1016/0079-6611(91)90004-6)
- Murray, J. W., Barber, R. T., Roman, M. R., Bacon, M. P., & Feely, R. A. (1994). Physical and biological controls on carbon cycling in the equatorial Pacific. *Science*, *266*(5182), 58–65. <https://doi.org/10.1126/science.266.5182.58>
- NASA Goddard Space Flight Center, Ocean Ecology Laboratory, Ocean Biology Processing Group. (2018a). *Moderate-Resolution Imaging Spectroradiometer (MODIS) Aqua Euphotic Depth Data; 2018 Reprocessing* [Data Set]. NASA OB.DAAC. <https://doi.org/10.5067/ORBVIEW-2/SEAWIFS/L3M/ZLEE/2018/10.5067/AQUA/MODIS/L3M/ZLEE/2018>
- NASA Goddard Space Flight Center, Ocean Ecology Laboratory, Ocean Biology Processing Group. (2018b). *Sea-Viewing Wide Field-of-View Sensor (SeaWiFS) Euphotic Depth Data; 2018 Reprocessing* [Data Set]. NASA OB.DAAC. <https://doi.org/10.5067/ORBVIEW-2/SEAWIFS/L3M/ZLEE/2018>
- Pennington, J. T., Mahoney, K. L., Kuwahara, V. S., Kolber, D. D., Calienes, R., & Chavez, F. P. (2006). Primary production in the eastern tropical Pacific: A review. *Progress in Oceanography*, *69*(2–4), 285–317. <https://doi.org/10.1016/j.pocean.2006.03.012>
- Pittman, N. A., Strutton, P. G., Johnson, R., & Matear, R. J. (2019). An assessment and improvement of satellite ocean color algorithms for the tropical Pacific Ocean. *Journal of Geophysical Research: Oceans*, *2019JC015498*. <https://doi.org/10.1029/2019JC015498>
- Plattner, G. K. (2005). Decoupling marine export production from new production. *Geophysical Research Letters*, *32*(11), L11612. <https://doi.org/10.1029/2005GL022660>
- Power, S., Lengaigne, M., Capotondi, A., Khodri, M., Vialard, J., Jebri, B., et al. (2021). Decadal climate variability in the tropical Pacific: Characteristics, causes, predictability, and prospects. *Science*, *374*. <https://doi.org/10.1126/science.aay9165>
- Quay, P. (1997). Was a carbon balance measured in the equatorial Pacific during JGOFS? *Deep Sea Research Part II: Topical Studies in Oceanography*, *44*(9–10), 1765–1781. [https://doi.org/10.1016/S0967-0645\(97\)00093-3](https://doi.org/10.1016/S0967-0645(97)00093-3)
- Racault, M. F., Sathyendranath, S., Brewin, R. J. W., Raitos, D. E., Jackson, T., & Platt, T. (2017). Impact of El Niño variability on oceanic phytoplankton. *Frontiers in Marine Science*, *4*. <https://doi.org/10.3389/fmars.2017.00133>
- Radenac, M. H., Léger, F., Singh, A., & Delcroix, T. (2012). Sea surface chlorophyll signature in the tropical Pacific during eastern and central Pacific ENSO events. *Journal of Geophysical Research*, *117*(C4).
- Radenac, M. H., Messié, M., Léger, F., & Bosc, C. (2013). A very oligotrophic zone observed from space in the equatorial Pacific warm pool. *Remote Sensing of Environment*, *134*, 224–233. <https://doi.org/10.1016/j.rse.2013.03.007>
- Raven, J. A., & Falkowski, P. G. (1999). Oceanic sinks for atmospheric CO₂. *Plant, Cell and Environment*, *22*(6), 741–755. <https://doi.org/10.1046/j.1365-3040.1999.00419.x>
- Reynolds, R. W., Rayner, N. A., Smith, T. M., Stokes, D. C., & Wang, W. (2002). An improved in situ and satellite SST analysis for climate. *Journal of Climate*, *15*(13), 1609–1625. [https://doi.org/10.1175/1520-0442\(2002\)015<1609:AIISAS>2.0.CO;2](https://doi.org/10.1175/1520-0442(2002)015<1609:AIISAS>2.0.CO;2)
- Roobaert, A., Laruelle, G. G., Landschützer, P., & Regnier, P. (2018). Uncertainty in the global oceanic CO₂ uptake induced by wind forcing: Quantification and spatial analysis. *Biogeosciences*, *15*(6), 1701–1720. <https://doi.org/10.5194/bg-15-1701-2018>
- Ryan, J. P., Polito, P. S., Strutton, P. G., & Chavez, F. P. (2002). Unusual large-scale phytoplankton blooms in the equatorial Pacific. *Progress in Oceanography*, *55*(3–4), 263–285. [https://doi.org/10.1016/S0079-6611\(02\)00137-4](https://doi.org/10.1016/S0079-6611(02)00137-4)
- Sabine, C. L., Feely, R. A., Johnson, G. C., Strutton, P. G., Lamb, M. F., & McTaggart, K. E. (2004). A mixed layer carbon budget for the GasEx-2001 experiment. *Journal of Geophysical Research*, *109*(C8). <https://doi.org/10.1029/2002JC001747>
- Sarmiento, J. L., & Gruber, N. (2006). *Ocean Biogeochemical Dynamics* (p. 103). Princeton University Press.
- Seager, R., Cane, M., Henderson, N., Lee, D. E., Abernathy, R., & Zhang, H. (2019). Strengthening tropical Pacific zonal sea surface temperature gradient consistent with rising greenhouse gases. *Nature Climate Change*, *9*(7), 517–522. <https://doi.org/10.1038/s41558-019-0505-x>
- Siegel, D. A., Buesseler, K. O., Doney, S. C., Saille, S. F., Behrenfeld, M. J., & Boyd, P. W. (2014). Global assessment of ocean carbon export by combining satellite observations and food-web models. *Global Biogeochemical Cycles*, *28*(3), 181–196. <https://doi.org/10.1002/2013GB004743>
- Silsbe, G. M., Behrenfeld, M. J., Halsey, K. H., Milligan, A. J., & Westberry, T. K. (2016). The CAFE model: A net production model for global ocean phytoplankton. *Global Biogeochemical Cycles*, *30*(12), 1756–1777. <https://doi.org/10.1002/2016GB005521>
- Strutton, P. G., & Chavez, F. P. (2000). Primary productivity in the equatorial Pacific during the 1997–1998 El Niño. *Journal of Geophysical Research*, *105*(C11), 26089–26101. <https://doi.org/10.1029/1999JC000056>
- Strutton, P. G., Chavez, F. P., Dugdale, R. C., & Hogue, V. (2004). Primary productivity in the central equatorial Pacific (3°S 130°W) during GasEx-2001. *Journal of Geophysical Research*, *109*(C8). <https://doi.org/10.1029/2003JC001790>
- Strutton, P. G., Evans, W., & Chavez, F. P. (2008). Equatorial Pacific chemical and biological variability, 1997–2003. *Global Biogeochemical Cycles*, *22*(2). <https://doi.org/10.1029/2007GB003045>
- Strutton, P. G., Palacz, A. P., Dugdale, R. C., Chai, F., Marchi, A., Parker, A. E., et al. (2011). The impact of equatorial Pacific tropical instability waves on hydrography and nutrients: 2004–2005. *Deep Sea Research Part II: Topical Studies in Oceanography*, *58*(3–4), 284–295. <https://doi.org/10.1016/j.dsr2.2010.08.015>
- Sutton, A. J., Feely, R. A., Maenner-Jones, S., Musielwicz, S., Osborne, J., Dietrich, C., et al. (2019). *Autonomous seawater pCO₂ and pH time series from 40 surface buoys and the emergence of anthropogenic trends* (Vol. 19). <https://doi.org/10.5194/essd-11-421-2019>
- Sutton, A. J., Feely, R. A., Sabine, C. L., McPhaden, M. J., Takahashi, T., Chavez, F. P., et al. (2014). Natural variability and anthropogenic change in equatorial Pacific surface ocean pCO₂ and pH. *Global Biogeochemical Cycles*, *28*(2), 131–145. <https://doi.org/10.1002/2013GB004679>
- Sutton, A. J., Sabine, C. L., Maenner-Jones, S., Lawrence-Slavas, N., Meinig, C., Feely, R. A., et al. (2014). *A high-frequency atmospheric and seawater pCO₂ data set from 14 open-ocean sites using a moored autonomous system* (Vol. 14). <https://doi.org/10.5194/essd-6-353-2014>
- Takahashi, T., Feely, R. A., Weiss, R. F., Wanninkhof, R. H., Chipman, D. W., & Sutherland, S. C. (1997). Global air-sea flux of CO₂: An estimate based on measurements of sea-air pCO₂ difference. *Proceedings of the National Academy of Sciences*, *94*(16), 8292–8299. <https://doi.org/10.1073/pnas.94.16.8292>

- Takahashi, T., Sutherland, S. C., Sweeney, C., Poisson, A., Metz, N., Tilbrook, B., et al. (2002). Global sea–air CO₂ flux based on climatological surface ocean pCO₂, and seasonal biological and temperature effects. *Deep Sea Research Part II: Topical Studies in Oceanography*, 49(9–10), 1601–1622. [https://doi.org/10.1016/S0967-0645\(02\)00003-6](https://doi.org/10.1016/S0967-0645(02)00003-6)
- Takahashi, T., Sutherland, S. C., Wanninkhof, R., Sweeney, C., Feely, R. A., Chipman, D. W., et al. (2009). Climatological mean and decadal change in surface ocean pCO₂, and net sea–air CO₂ flux over the global oceans. *Deep Sea Research Part II: Topical Studies in Oceanography*, 56(8–10), 554–577. <https://doi.org/10.1016/j.dsr2.2008.12.009>
- Turk, D., Lewis, M. R., Harrison, G. W., Kawano, T., & Asanuma, I. (2001). Geographical distribution of new production in the western/central equatorial Pacific during El Niño and non-El Niño conditions. *Journal of Geophysical Research*, 106(C3), 4501–4515. <https://doi.org/10.1029/1999JC000058>
- Turk, D., Meinen, C., Antoine, D., McPhaden, M., & Lewis, M. (2011). Implications of changing El Niño patterns for biological dynamics in the equatorial Pacific Ocean. *Geophysical Research Letters*, 38(23). <https://doi.org/10.1029/2011GL049674>
- Turk, D., Zappa, C. J., Meinen, C. S., Christian, J. R., Ho, D. T., Dickson, A. G., & McGillis, W. R. (2010). Rain impacts on CO₂ exchange in the western equatorial Pacific Ocean. *Geophysical Research Letters*, 37(23). <https://doi.org/10.1029/2010GL045520>
- Valsala, V. K., Roxy, M. K., Ashok, K., & Murtugudde, R. (2014). Spatiotemporal characteristics of seasonal to multidecadal variability of pCO₂ and air–sea CO₂ fluxes in the equatorial Pacific Ocean. *Journal of Geophysical Research: Oceans*, 119(12), 8987–9012. <https://doi.org/10.1002/2014jc010212>
- Wanninkhof, R., & Triñanes, J. (2017). The impact of changing wind speeds on gas transfer and its effect on global air–sea CO₂ fluxes: Impact of Changing Winds on CO₂ Fluxes. *Global Biogeochemical Cycles*, 31(6), 961–974. <https://doi.org/10.1002/2016GB005592>
- Weiss, R. F. (1974). Carbon dioxide in water and seawater: The solubility of a non-ideal gas. *Marine Chemistry*, 2(3), 203–215. [https://doi.org/10.1016/0304-4203\(74\)90015-2](https://doi.org/10.1016/0304-4203(74)90015-2)
- Weller, E., Min, S. K., Cai, W., Zwiers, F. W., Kim, Y. H., & Lee, D. (2016). Human-caused Indo-Pacific warm pool expansion. *Science Advances*, 2(7), e1501719. <https://doi.org/10.1126/sciadv.1501719>
- Wentz, F. J., Scott, J., Hoffner, R., Leidner, M., & Ardizzone, J. (2015). *Remote Sensing Systems Cross-Calibrated Multi-Platform (CCMP) 6-Hourly Ocean Vector Wind Analysis Product on 0.25° Grid, Version 2.0* [Data Set]. Remote Sensing Systems. Retrieved from www.remss.com/measurements/ccmp
- Westberry, T., Behrenfeld, M. J., Siegel, D. A., & Boss, E. (2008). Carbon-based primary productivity modeling with vertically resolved photoacclimation: CARBON-BASED production model. *Global Biogeochemical Cycles*, 22(2). <https://doi.org/10.1029/2007GB003078>
- Wyrki, K. (1981). An estimate of equatorial upwelling in the Pacific. *Journal of Physical Oceanography*, 11(9), 1205–1214. [https://doi.org/10.1175/1520-0485\(1981\)011<1205:AEOEUI>2.0.CO;2](https://doi.org/10.1175/1520-0485(1981)011<1205:AEOEUI>2.0.CO;2)
- Yasunaka, S., Kouketsu, S., Strutton, P. G., Sutton, A. J., Murata, A., Nakaoka, S., & Nojiri, Y. (2019). Spatio-temporal variability of surface water pCO₂ and nutrients in the tropical Pacific from 1981 to 2015. *Deep Sea Research Part II: Topical Studies in Oceanography*, 169–170, 104680. <https://doi.org/10.1016/j.dsr2.2019.104680>
- Yeh, S. W., Kug, J. S., Dewitte, B., Kwon, M. H., Kirtman, B. P., & Jin, F. F. (2009). El Niño in a changing climate. *Nature*, 461(7263), 511–514. <https://doi.org/10.1038/nature08316>